SCATTERING FROM COATED STRUCTURES AND ANTENNA PATTERN CONTROL USING IMPEDANCE SURFACES

Semiannual Progress Report

PART A

Constantine A. Balanis and Lesley A. Polka

February 1, 1990 - July 31, 1990

PART B

Constantine A. Balanis and Kefeng Liu

February 1, 1990 - July 31, 1990

Telecommunications Research Center
Department of Electrical Engineering
Arizona State University
Tempe, Arizona 85287-7206

Grant No. NAG-1-562
National Aeronautics and Space Administration
Langley Research Center
Hampton, VA 23665

PART A

SCATTERING FROM COATED STRUCTURES

ABSTRACT

Part A of this report examines the scattering from coated, conducting structures, specifically the coated dihedral corner reflector configuration and the coated strip/plate configuration. The formulation uses impedance-wedge Uniform Theory of Diffraction scattering coefficients to calculate the diffracted fields. A finite-thickness coating is approximated using the impedance boundary condition to arrive at an equivalent impedance for the coating. The formulation of the impedance wedge coefficients is outlined. Far-field, perfectly conducting approximations are discussed. Problems with the present dihedral corner reflector model for certain angles of incidence and observation are discussed along with a potentially rectifying modification. Because the interactions involved in analyzing the scattering from a dihedral corner reflector are quite complicated, the strip/plate model is developed as a simpler configuration for analyzing the diffraction coefficient modifications and for isolating problem areas. Comparisons with data obtained experimentally and using the Finite-Difference Time-Domain method are included for the plate geometry.

I. INTRODUCTION

Now that high-frequency techniques for perfectly conducting geometries, such as the UTD [1], [2] and various equivalent currents methods [3]-[10], have reached a mature stage of development, the emphasis in the research on high-frequency techniques has shifted to dielectric and dielectric-covered materials. Dielectric materials are useful in radar cross section (RCS) reduction, thus accurate prediction techniques are necessary for modeling procedures. Just as in the perfectly conducting case, the wedge geometry is the canonical structure used to determine scattering coefficients. Maliuzhinets presented an exact solution to the scattering by an impedance wedge at normal incidence in 1958 [11]; however, the difficult mathematical nature of the representation precluded easy analytical use of the solution.

Recent work has concentrated on asymptotic approximations to Maliuzhinets' exact solution in order to obtain computationally tractable methods for predicting impedance-wedge scattering. Initial solutions were for limited cases, such as the half-plane and 90-degree wedge. In 1967, Bowman [12] used a steepest-descent approximation to Maliuzhinets' wedge solution for the special case of a half-plane configuration to determine the scattering from an infinite impedance strip. This solution was limited to normal-incidence backscattering and was non-uniform [13]. In other words, this solution was analogous to using Keller's GTD diffraction coefficients [1] for the perfectly conducting wedge.

More recent work by Tiberio, Pelosi, and Manara [13] has extended to a uniform solution for first-order scattering from an infinite strip at grazing incidence, analogous to the use of the UTD diffraction coefficients [2] for the perfectly conducting wedge. This work also considered higher-order scattering due to edge interactions by using an extended spectral method, analogous to previous work in the perfectly conducting realm [14]-[16]. In an extension of this work, Tiberio and Pelosi later considered the scattering from impedance discontinuities in a flat, infinite plane [17].

In a parallel attempt to formulate high-frequency approximations to impedance wedge scattering, Volakis derived uniform diffraction coefficients for scattering at normal and oblique incidence from an impedance half-plane using a Wiener-Hopf solution to impedance half-plane scattering [18]. The resulting coefficients were similar to the UTD coefficients for perfectly conducting geometries and were just as computationally efficient because the integrals involved in the solution were numerically approximated. In later work, Senior and Volakis presented similar solutions for a 90-degree imperfectly conducting wedge with one impedance face and one perfectly conducting face [19] and for a dielectric half-plane of a given thickness [20]. Herman and Volakis also derived coefficients for up to third-order diffractions from resistive, conductive, and impedance strips for all angles of incidence and observation [21]. Volakis generalized this work in his solution for scattering from finite-thickness impedance half-planes and strips [22] which involved a dual-integral equation solution and the extended spectral ray method.

Most of the recent accomplishments in the area of impedance wedge scattering theory have been limited to special cases. In 1985, however, Tiberio, Pelosi, and Manara presented a general high-frequency formulation for Maliuzhinets' impedance wedge solution in the form of a diffraction coefficient that was analogous to the perfectly conducting UTD diffraction coefficient [23]. This solution contained the computationally inefficient Maliuzhinets function that prevented obtaining numerical results for all but the 180-, 270-, and 360-degree impedance wedges. The UTD formulation, however, was very promising if an accurate, generalized method for computing the Maliuzhinets function could be formulated.

Recently, Griesser and Balanis reported a new, computationally efficient, representation for the geometrical optics and diffraction terms for impedance-wedge scattering [24] based upon the UTD formulation of Tiberio, Pelosi, and Manara [23]. Using a series of identities, the geometrical optics term is represented in terms of reflection coefficients as opposed to Maliuzhinets functions, greatly simplifying numerical computations. Additionally, the efficiency of the UTD diffraction coefficient is improved by representing a double integral in the complex plane in terms of the product of eight single integrals in the real plane, which can be easily and quickly evaluated with standard numerical integration routines. The results for impedance wedges are highly accurate, as Griesser and Balanis reported [24]; and the solution allows easy and fast computation of the scattered fields for any size impedance wedge, not just certain cases as in the past. The relative computational ease with which the diffraction coefficients for any size impedance wedge can be

calculated allows the high-frequency modeling of more complicated geometries such as the impedance dihedral corner reflector, which has been analyzed in a previous report [25] and in [26].

A more interesting target configuration than one composed of a homogeneous material is a coated conductor target, which could realistically be found in low-observable vehicle designs. The main problem in modeling a coated-conductor target is in representing the effects of a finite-thickness coating. Research in this area is in the incipient stages. Newman and Schrote use an approximate boundary condition at normal incidence, which is essentially a transmission line equivalent impedance, in their Moment Method (MM) solution [27]. Jin and Liepa also use this approximation in their numerical method for computing the scattering from coated wedges illuminated by a TM plane wave [28]. Although Senior is investigating solutions for coated geometries involving higher-order boundary conditions [29], the approximate first-order boundary condition is much simpler to apply and to use computationally; thus this is the boundary condition analyzed in this report.

In their initial investigation of coated dihedral corner reflectors [25] and [26], Griesser and Balanis use the approximate boundary condition at normal incidence. This speeds up the computation time by eliminating the calculation of a new equivalent impedance at each incidence angle. For the higher-order terms included in the dihedral corner reflector model, this would be a complicated task. In the last report [30], however, it was stated that using the normal incidence transmission line impedance model for a finite-coating thickness is insufficient except for highly

conductive coatings or near and at normal incidence to either one of the plates composing the corner reflector. This report details the latest investigations concerning the improvement of the present model for the coated dihedral corner reflector. After a brief discussion of the UTD impedance wedge diffraction coefficient and the corner reflector model, a formulation for the coated strip/plate model is presented along with numerical results. The strip/plate model is a much simpler target to analyze in terms of isolating and identifying key factors in finite-thickness coating modeling; thus it is an important point at which to begin in improving the present dihedral corner reflector model.

II. THEORY AND RESULTS

A. IMPEDANCE-WEDGE DIFFRACTION COEFFICIENT

The fields diffracted from an impedance wedge at a distance ρ from the wedge configuration of Fig. 1 can be represented as:

$$E^d(\rho) = E^i(Q)\ D(\phi, \phi, \theta_o, \theta_n, k\rho)\ e^{-jk\rho} / \sqrt{\rho} \qquad (1)$$

where

$E^i(Q)$ = incident field at the point of diffraction due to plane-wave incidence

$D(\phi, \phi', \theta_o, \theta_n, k\rho)$ = impedance-wedge diffraction coefficient

ϕ = diffraction angle

ϕ' = incidence angle

θ_o = Brewster angle for the "o" face

θ_n = Brewster angle for the "n" face

ρ = distance from the diffraction point to the observation point

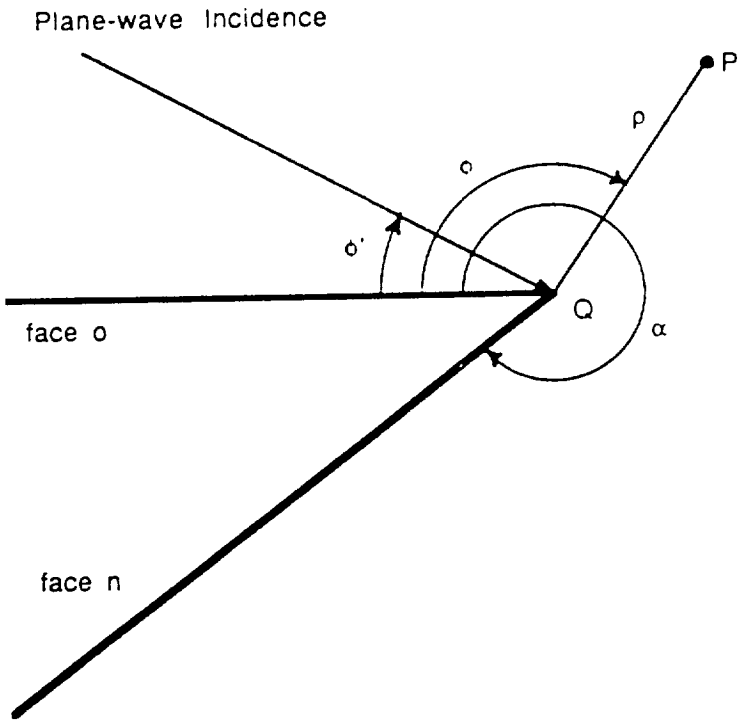

Fig. 1. Impedance wedge geometry.

Far-field observation of line-source diffraction can be incorporated by reciprocity. The wedge configuration is illustrated in Fig. 1. The explicit form of the diffraction coefficient is in [23] and will not be repeated here. The diffraction coefficient consists of various factors including reflection coefficient factors, Fresnel transition function factors, and a factor containing the $M_n(\phi,\phi',\theta_o)$ Maliuzhinets function, which consists of a nested double integral in the complex plane. Griesser and Balanis present a simplification of this function in [24] which allows easy calculation of the diffraction coefficient for any size impedance wedge.

The items of interest in the analysis for coated conducting surfaces are the Brewster angles, θ_o and θ_n. These are defined as:

Soft Polarization:

$$\theta_o = \sin^{-1}(1/\eta_o) \tag{2}$$

$$\theta_n = \sin^{-1}(1/\eta_n) \tag{3}$$

Hard Polarization:

$$\theta_o = \sin^{-1}(\eta_o) \tag{4}$$

$$\theta_n = \sin^{-1}(\eta_n) \tag{5}$$

where

η_o = surface impedance of face "o", normalized with respect to the free-space impedance

η_n = surface impedance of face "n", normalized with respect to the free-space impedance

The surface impedance for a finite-thickness coating is discussed in the following section. For a coated conductor, the "n" face is a perfect conductor, which has a surface impedance of zero. This presents problems in numerical calculations because the corresponding Brewster angle for soft polarization is infinite and for hard polarization is 0. A means of avoiding computational errors is to

represent the perfectly conducting surface with a small but non-zero surface impedance. Comparisons between the fields diffracted by a perfectly conducting half-plane, calculated using the perfectly conducting UTD coefficients [2], and the fields diffracted by various impedance half-planes with non-zero surface impedances, calculated using the impedance-wedge diffraction coefficients [24], are shown in Figs. 2 - 7. For bistatic scattering, using η = 0.00001 to approximate a perfectly conducting surface is an adequate, but not perfect, approximation for both polarizations (Fig. 2 and Fig. 5). For monostatic scattering near-field incidence, the approximation improves (Fig. 3 and Fig. 6). Finally, for monostatic plane-wave scattering far-field observation, which is the type of scattering considered for RCS prediction, the η = 0.00001 approximation produces nearly identical results to the perfectly conducting geometry (Fig. 4 and Fig. 7). This approximation will, therefore, be used in the remainder of this analysis.

B. EQUIVALENT SURFACE IMPEDANCE FOR A COATED CONDUCTOR

The shorted, transmission-line impedance is a standard approximation for the equivalent impedance of a conductor with a finite-thickness coating [31]. The equivalent impedance normalized to the free-space impedance is:

$$\eta_{eq} = j\eta \tan(kt \sin(\phi_t)) \tag{6}$$

where

$\eta = \sqrt{\mu_c / \varepsilon_c}$

$k = \omega \sqrt{\mu\varepsilon}$

t = the coating thickness

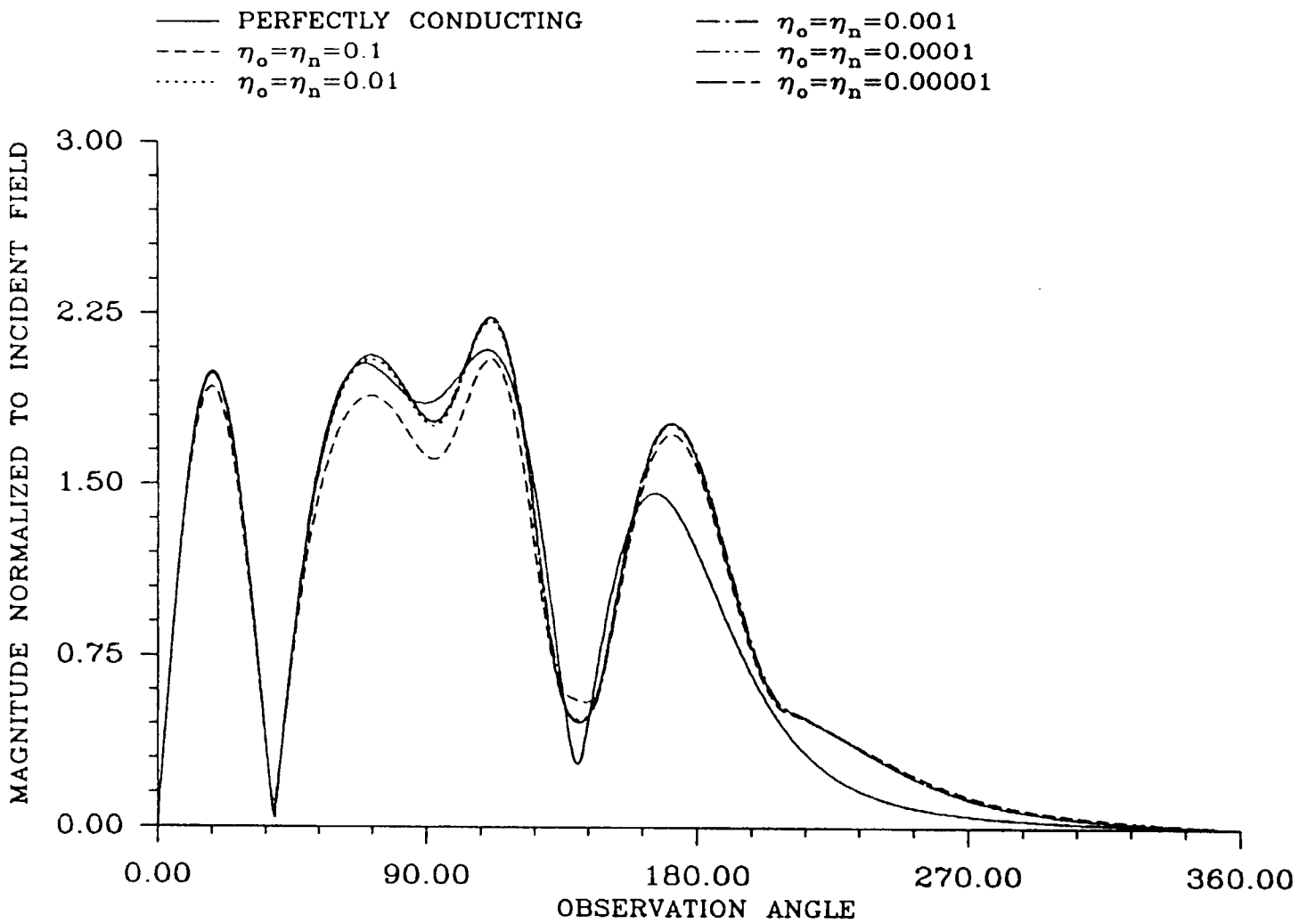

Fig. 2. Bistatic impedance-wedge scattering (α = 360°, ϕ' = 30°, ρ = 1.6 λ, soft polarization).

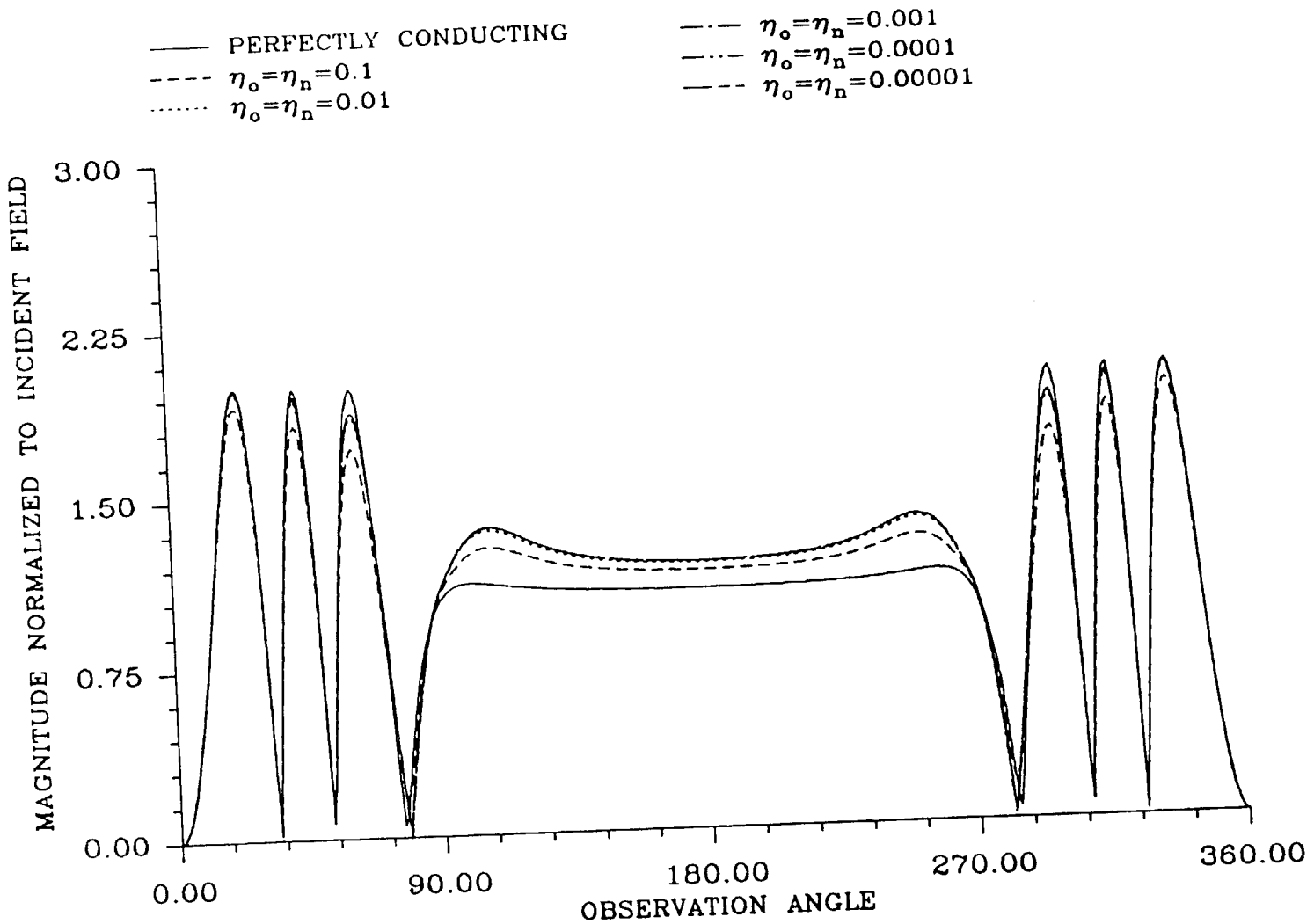

Fig. 3. Monostatic impedance-wedge scattering ($\alpha = 360^\circ$, $\rho = 1.6\ \lambda$, soft polarization).

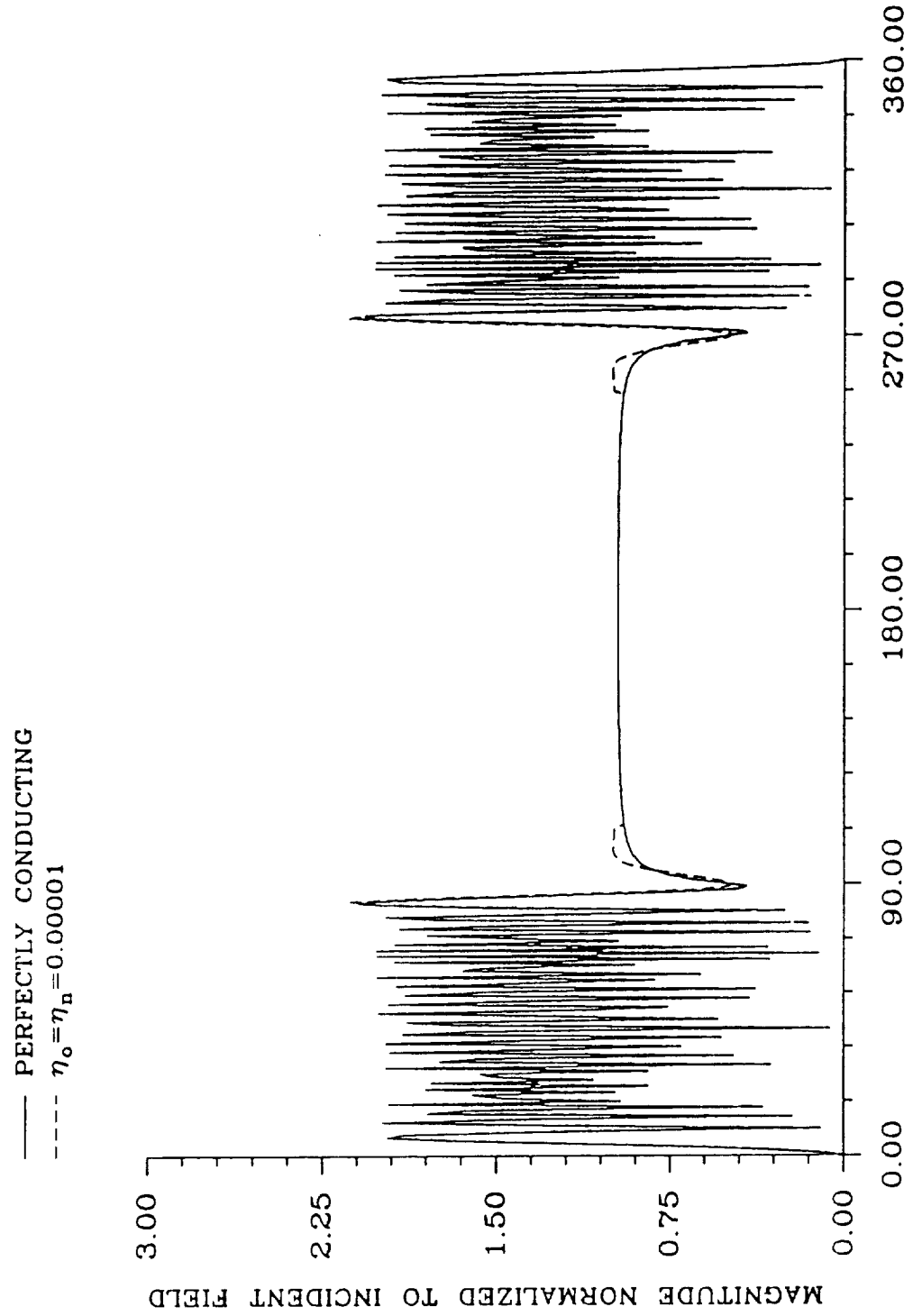

Fig. 4. Monostatic impedance-wedge scattering (α = 360°, ρ = 20 λ, soft polarization).

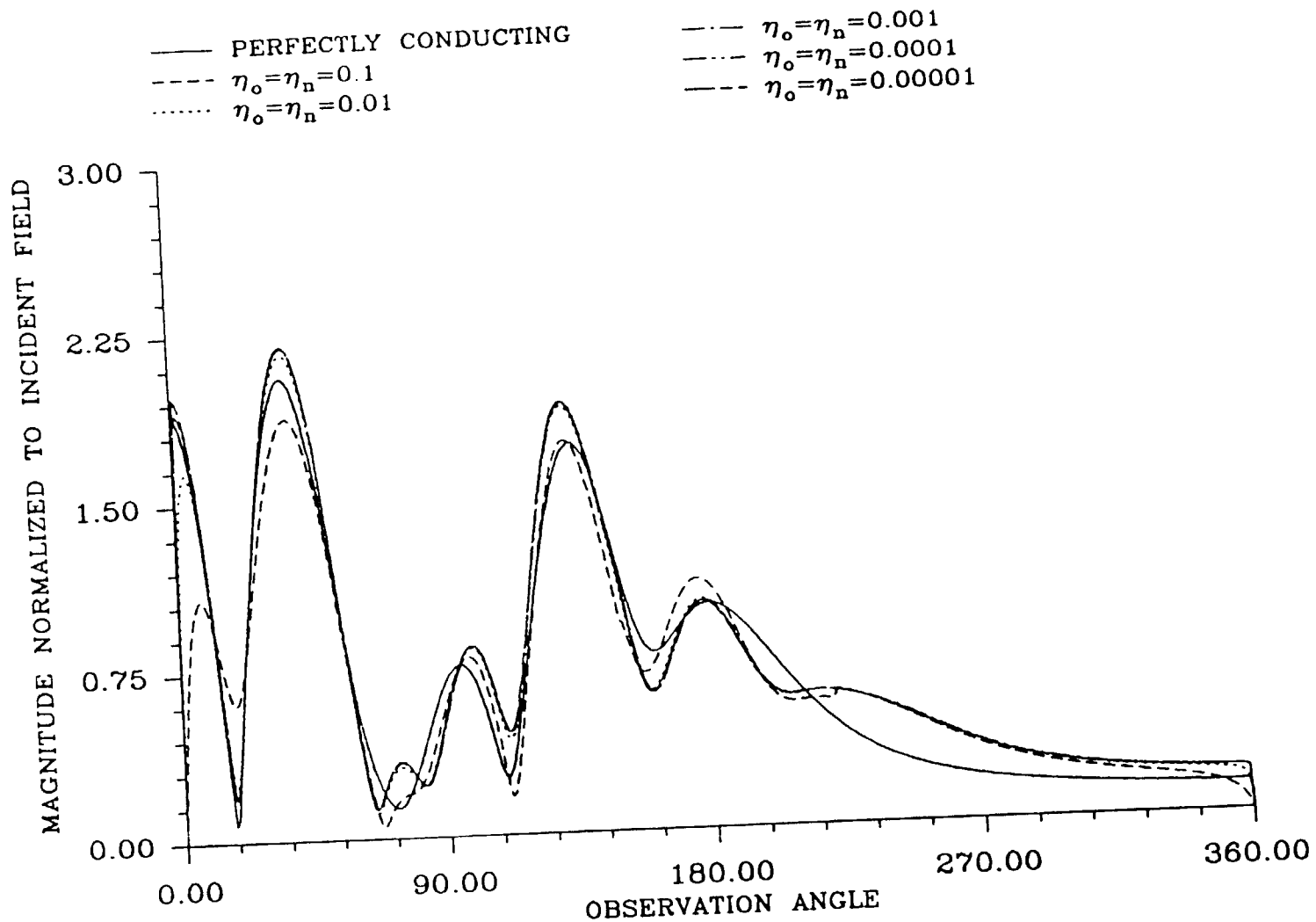

Fig. 5. Bistatic impedance-wedge scattering (α = 360°, ϕ' = 30°, ρ = 1.6 λ, hard polarization).

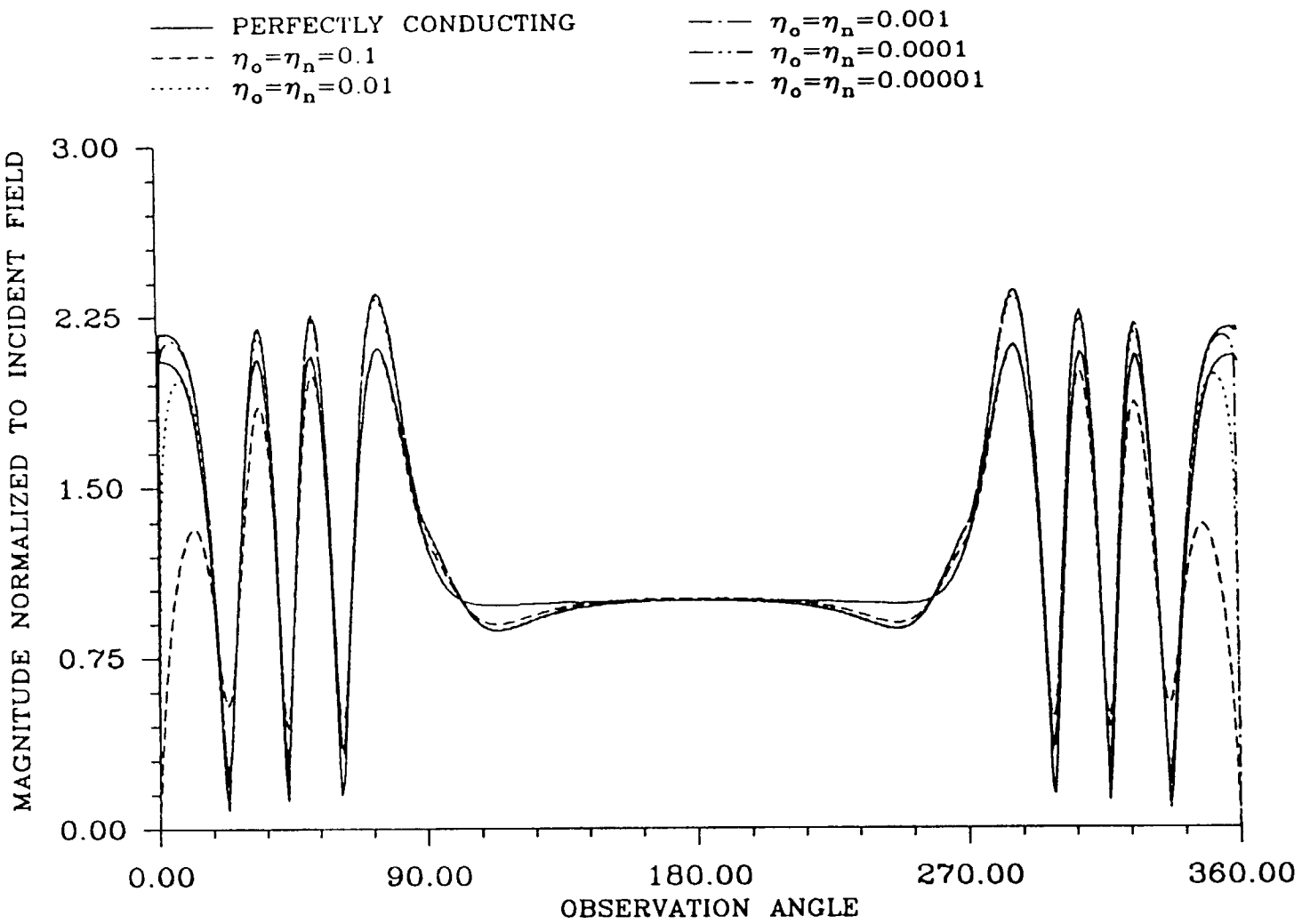

Fig. 6. Monostatic impedance-wedge scattering (α = 360°, ρ = 1.6 λ, hard polarization).

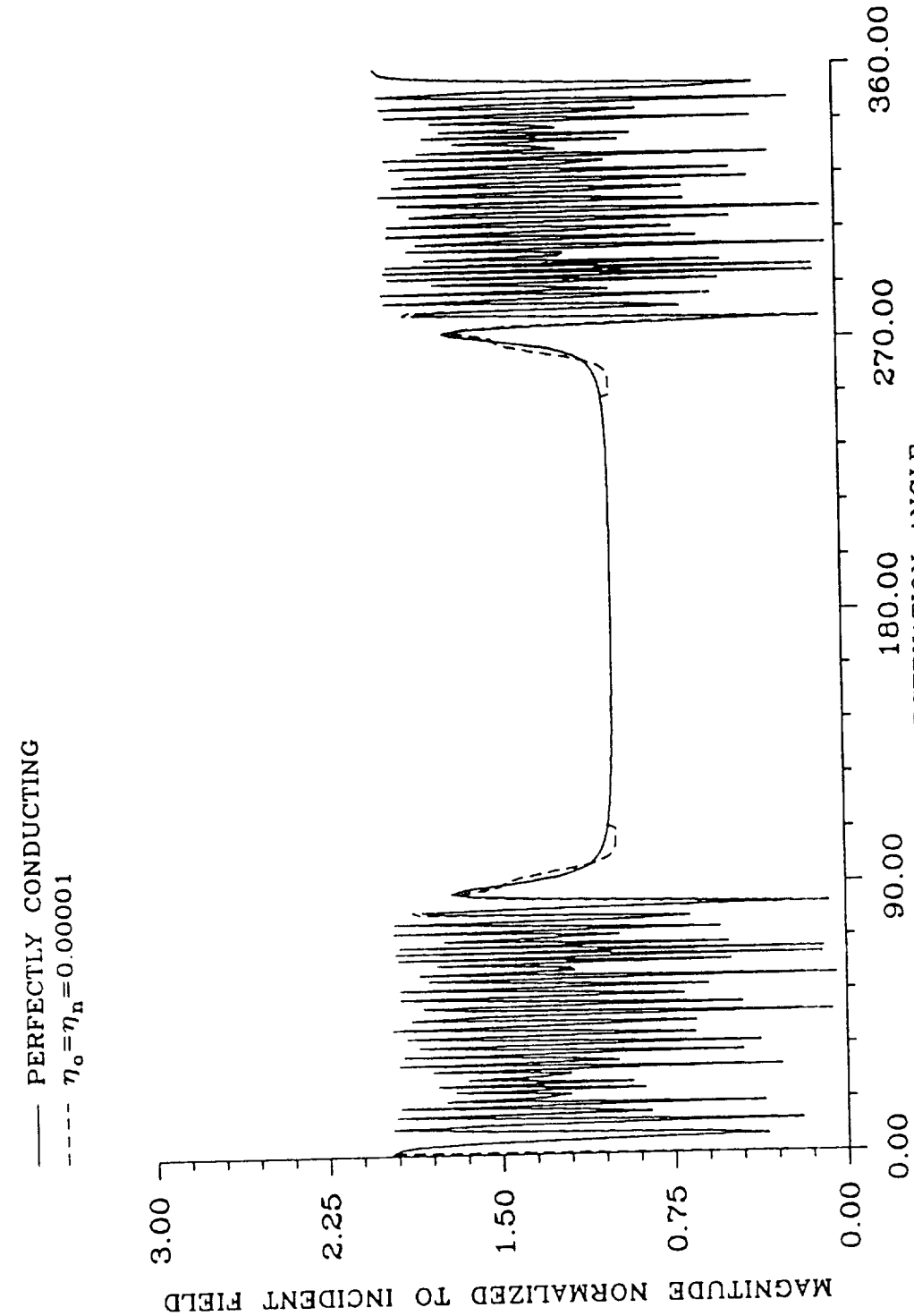

Fig. 7. Monostatic impedance-wedge scattering ($\alpha = 360^\circ$, $\rho = 20\ \lambda$, hard polarization).

μ_c, ε_c = the relative permeability and relative permittivity of the coating

μ, ε = the permeability and permittivity of the coating

ϕ_t = the angle of the transmitted ray with respect to the surface of the coating

It is a standard practice to use the equivalent impedance calculated at normal incidence, $\phi_t = 90^\circ$. This is valid provided that either the incidence angle is near or at normal, or that the coating has a high permittivity or a high conductivity, or that the coating is very thin compared to a wavelength.

C. COATED DIHEDRAL CORNER REFLECTOR

The equivalent surface impedance for the coated dihedral corner reflector (Fig. 8) was originally approximated by setting $\phi_t = 90^\circ$ [25]. The results compare favorably with MM results for high conductivity coatings and for angles near normal incidence. For less conductive materials and for angles away from normal incidence to one of the plates comprising the reflector the accuracy declines. Fig. 9 compares MM results with UTD results for one of the worst cases, the 90° corner reflector. In an initial attempt to correct the UTD model, an angularly varying equivalent impedance was incorporated into the first-order reflection terms only as these were thought to be the most significant terms in error. The angularly varying equivalent impedance was not included in the diffracted terms. A pattern computed based on this model is shown in Fig. 10 along with the UTD results from Fig. 9 using the original model. The two models give nearly identical results. This indicates that the angular dependence of the equivalent impedance in the reflected terms does not play a

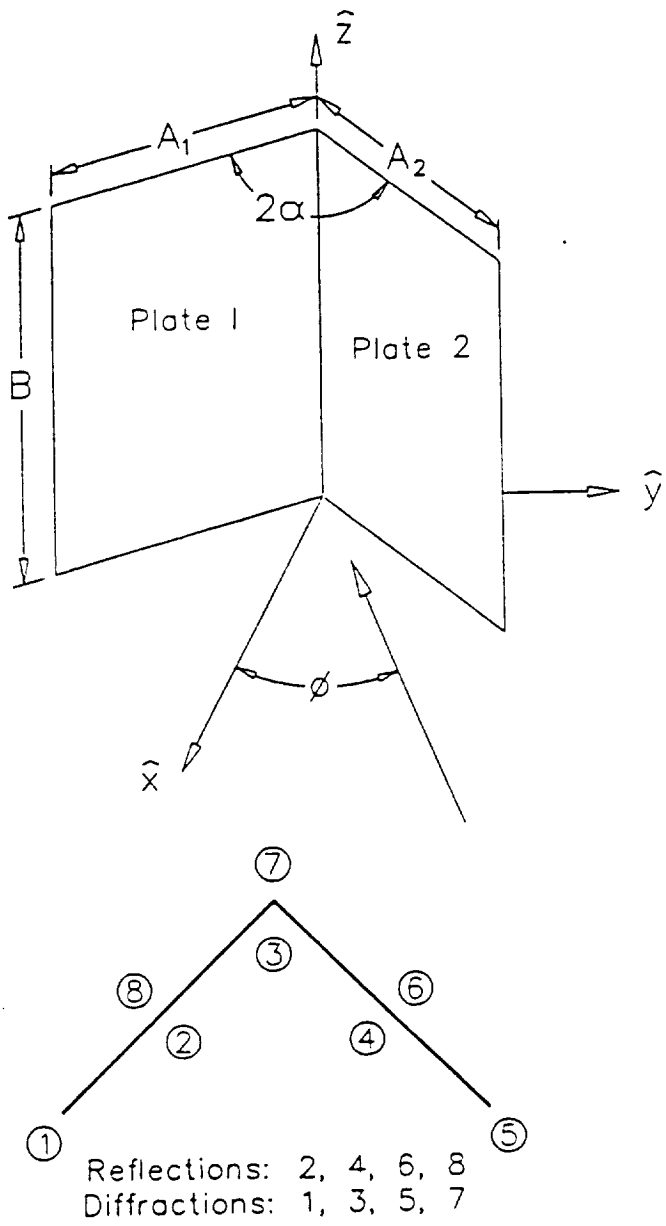

Fig. 8. Coated dihedral corner reflector geometry.

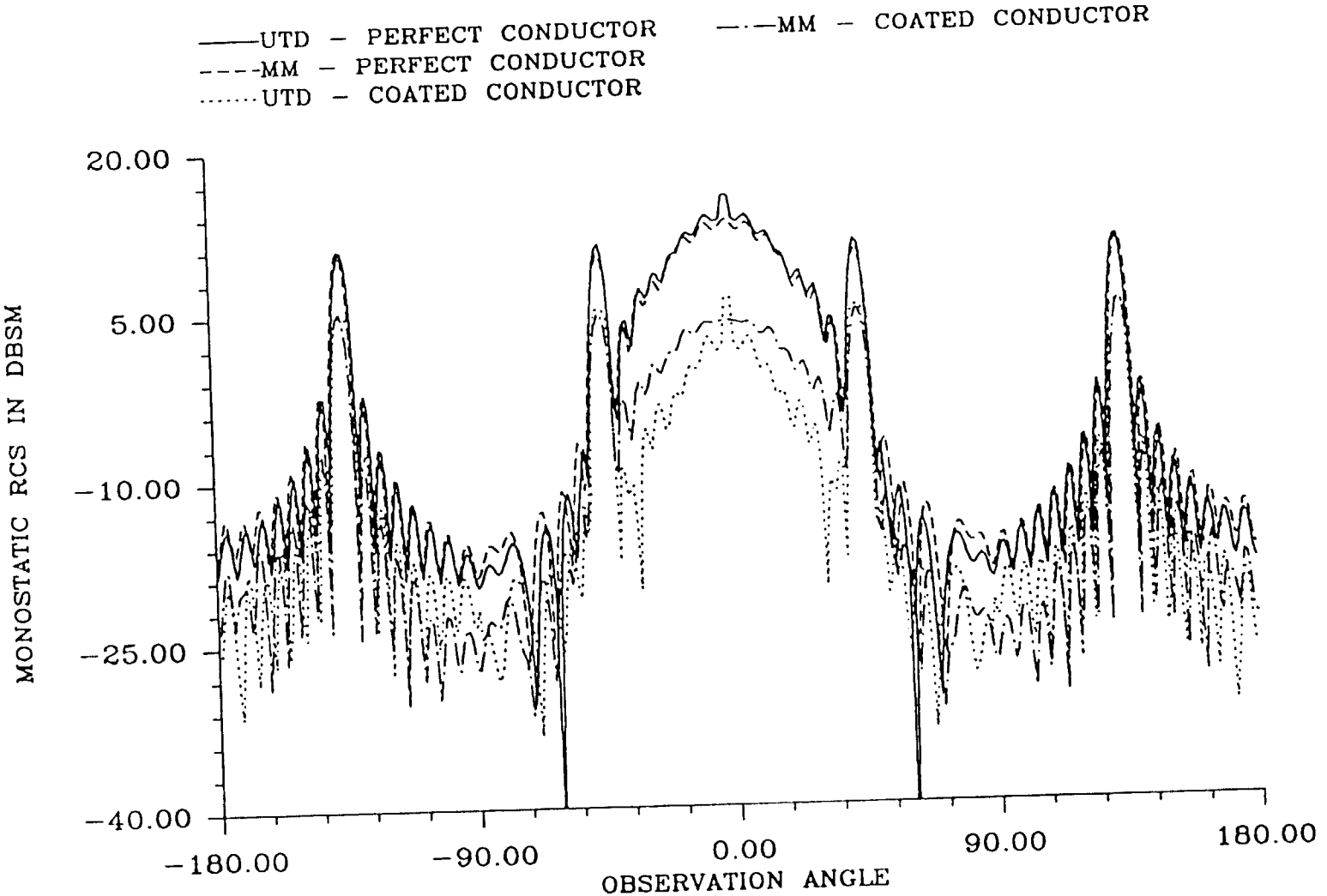

Fig. 9. Monostatic RCS of a perfectly conducting and a coated 90° dihedral corner reflector (soft polarization, $2\alpha = 90^{\circ}$, A1 = A2 = B = 5.6088 λ, coating: $\varepsilon_c = 7.8 - j1.6$, $\mu_c = 1.5 - j0.7$, $t = 0.052\ \lambda$).

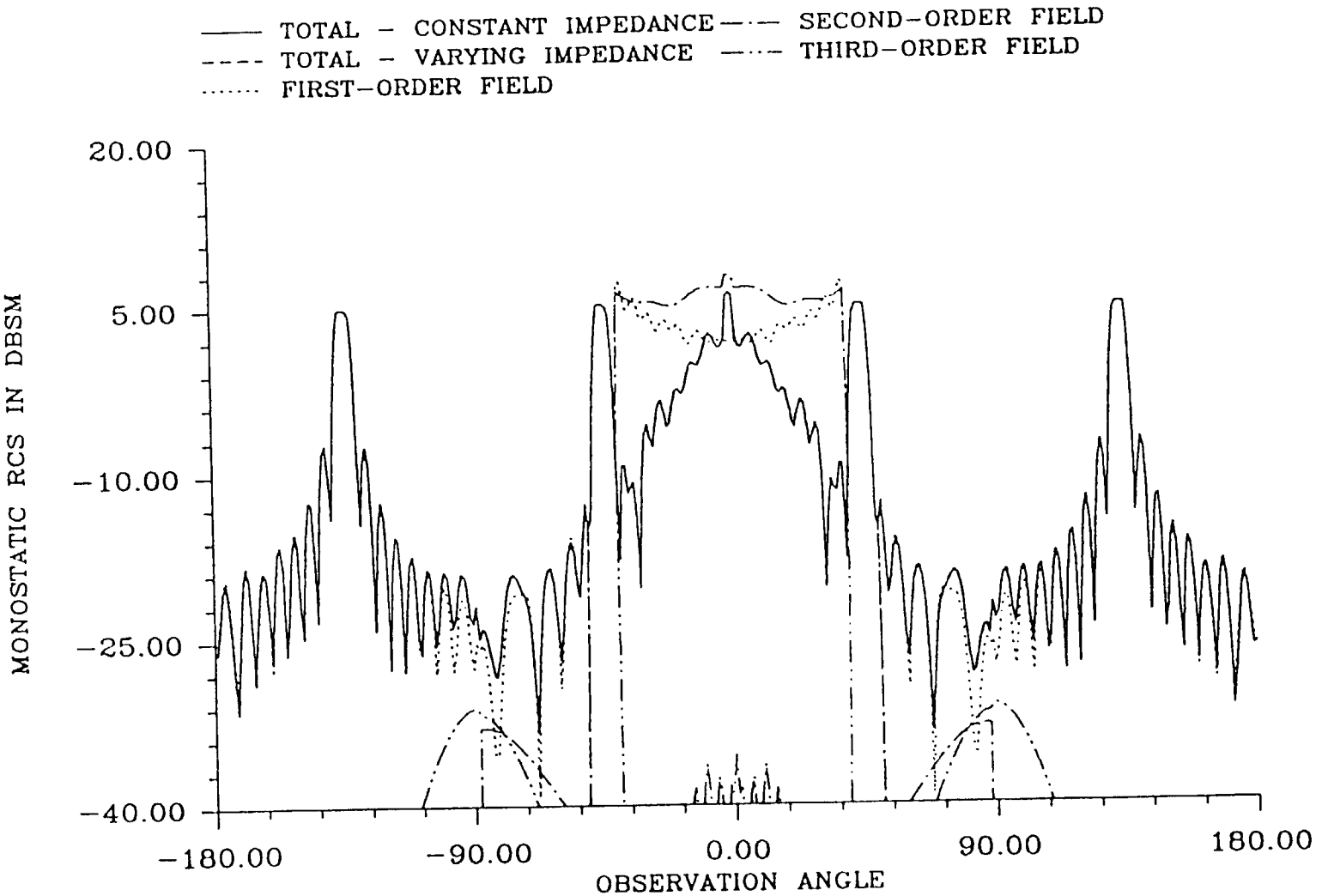

Fig. 10. Monostatic scattering components of a 90° dihedral corner reflector (soft polarization, $2\alpha = 90^{\circ}$, $\varepsilon_c = 7.8 - j1.6$, $\mu_c = 1.5 - j0.7$, $t = 0.052\ \lambda$, $A1 = A2 = B = 5.6088\ \lambda$).

major role; however, this may not be the case for the diffracted terms.

An analysis of the various higher-order scattering terms reveals that the most significant terms in the areas of disagreement are first-order and second-order terms involving diffraction. This is illustrated in Figs. 10 - 14 which contain a breakdown of the individual terms. The nomenclature used is:

Hn - first-order diffraction or reflection from point "n"

Hnm - second-order diffraction-diffraction, reflection-diffraction, diffraction-reflection, or reflection-reflection from n to m

Incorporating the angularly varying surface impedance into diffraction terms of the dihedral corner reflector model is a complicated task; and it is postponed for the next period and until an evaluation of the scattering from a coated plate is complete, where this variation will be investigated.

D. COATED, RECTANGULAR PLATE

Because of its simplicity, the coated, rectangular plate of Fig. 15 is a convenient configuration for studying the effects of an angularly varying equivalent surface impedance approximation for the finite-thickness coating. At present, the model contains first-order diffraction terms only. Comparisons between the UTD results obtained with a constant equivalent surface impedance calculated at normal incidence and UTD results obtained with an angularly varying impedance are shown in Figs. 16 and 17. The Finite-Difference Time-Domain (FD-TD) method is used for comparison in Fig. 16, and experimental data is used in Fig. 17. Near normal incidence the two UTD methods

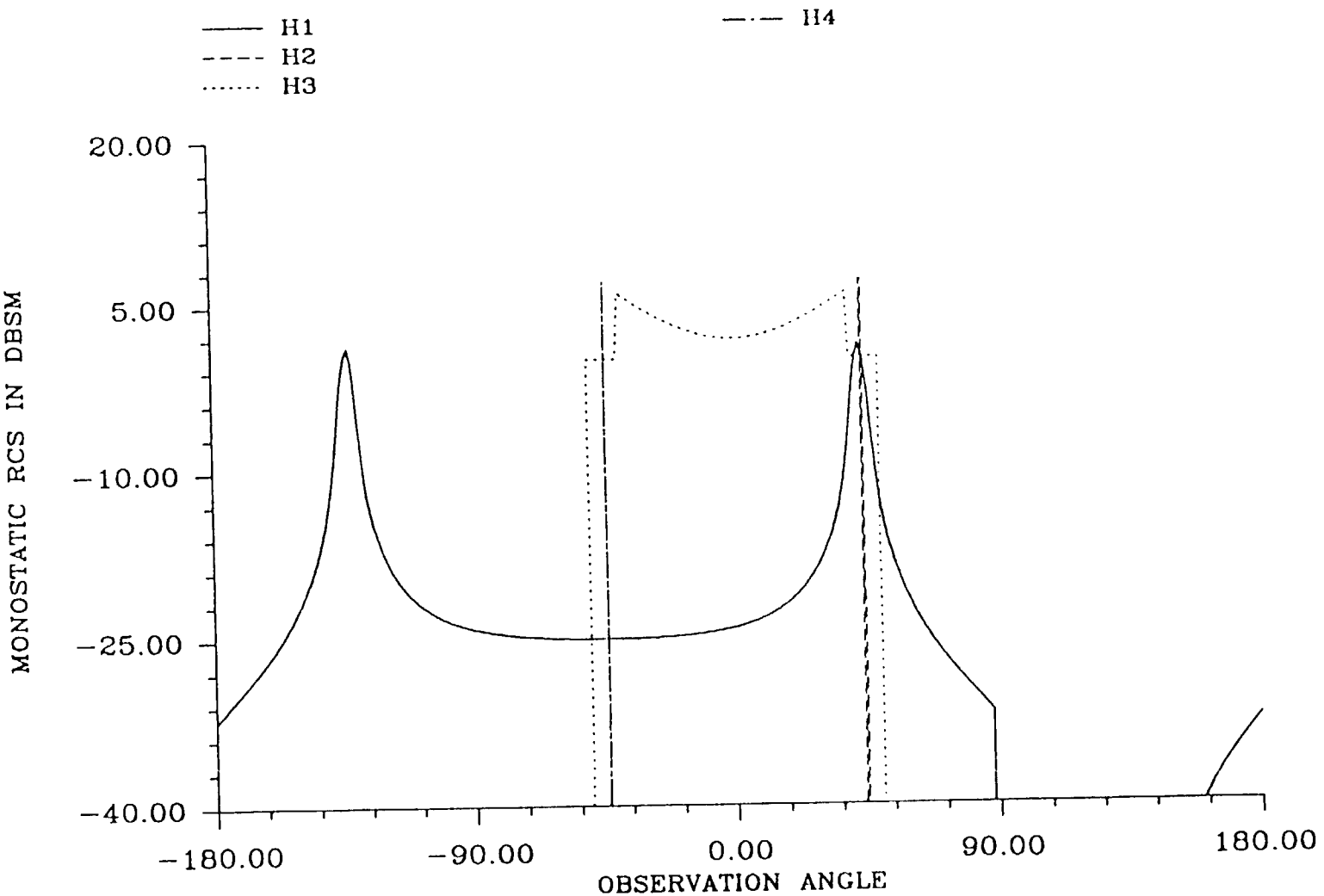

Fig. 11. Monostatic scattering components of a 90° dihedral corner reflector (soft polarization, $2\alpha = 90^{\circ}$, $\varepsilon_c = 7.8 - j1.6$, $\mu_c = 1.5 - j0.7$, $t = 0.052\ \lambda$, $A1 = A2 = B = 5.6088\ \lambda$).

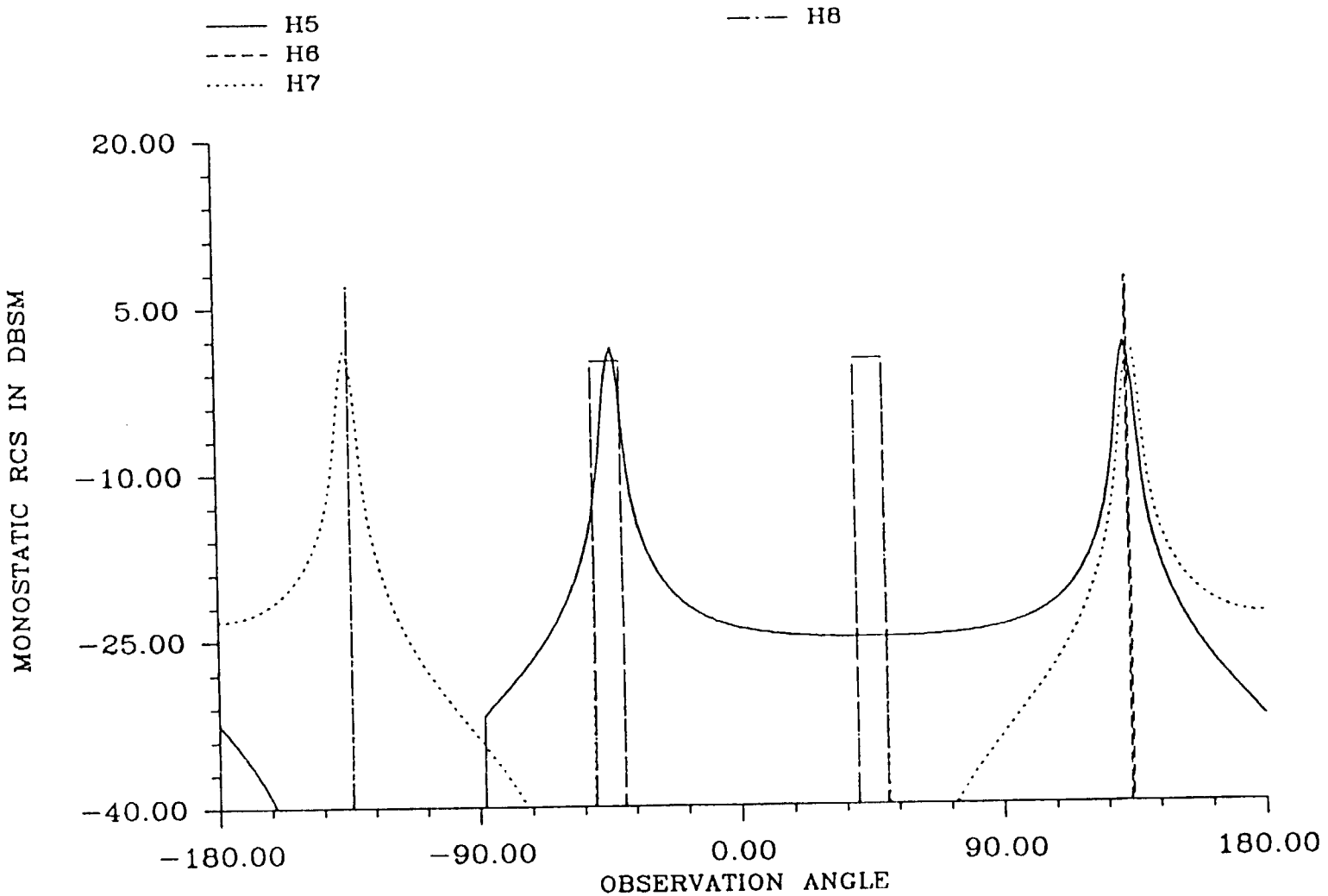

Fig. 12. Monostatic scattering components of a 90° dihedral corner reflector (soft polarization, $2\alpha = 90^{\circ}$, $\varepsilon_c = 7.8 - j1.6$, $\mu_c = 1.5 - j0.7$, $t = 0.052\ \lambda$, $A1 = A2 = B = 5.6088\ \lambda$).

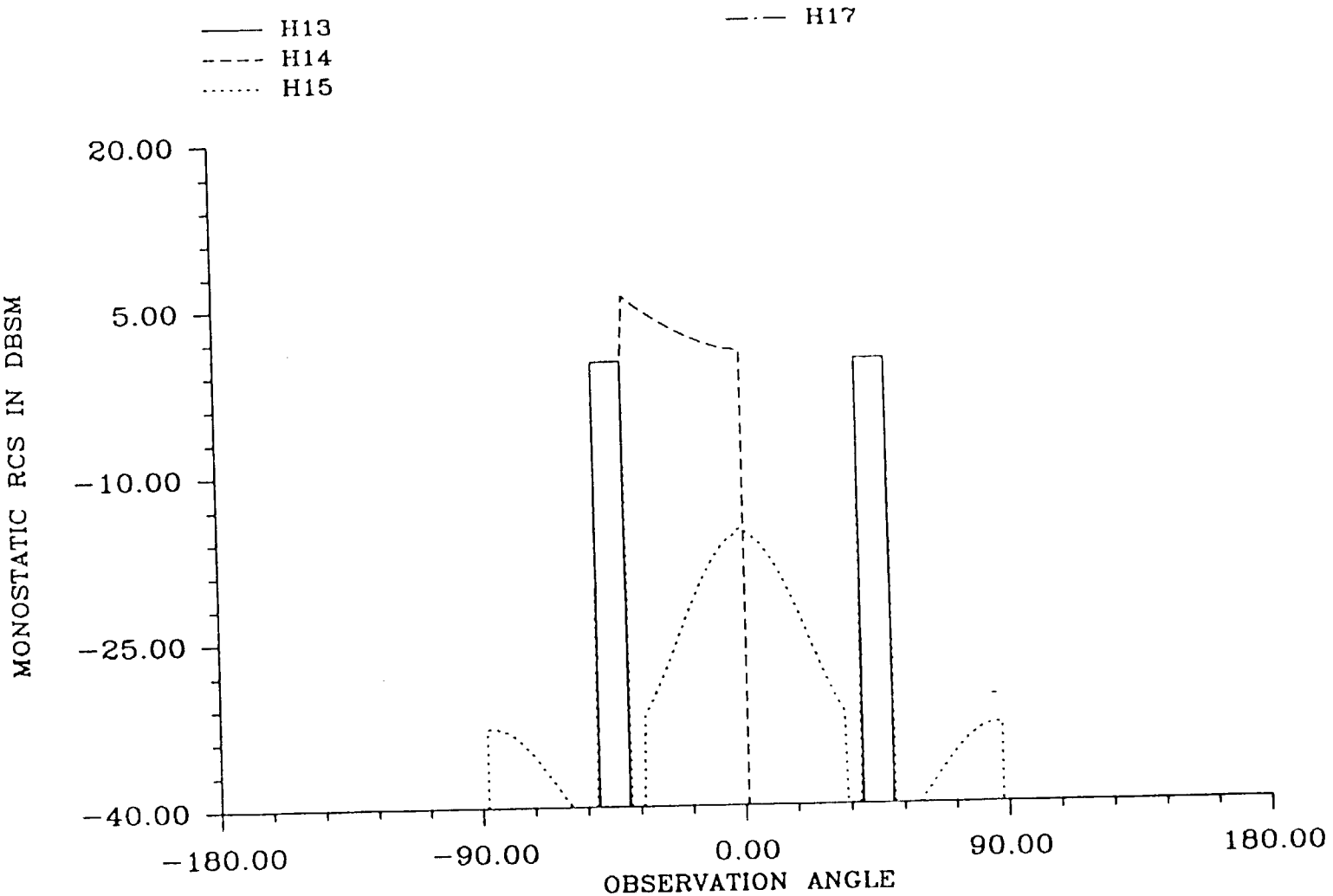

Fig. 13. Monostatic scattering components of a 90° dihedral corner reflector (soft polarization, $2\alpha = 90^{\circ}$, $\varepsilon_c = 7.8 - j1.6$, $\mu_c = 1.5 - j0.7$, $t = 0.052\ \lambda$, $A1 = A2 = B = 5.6088\ \lambda$).

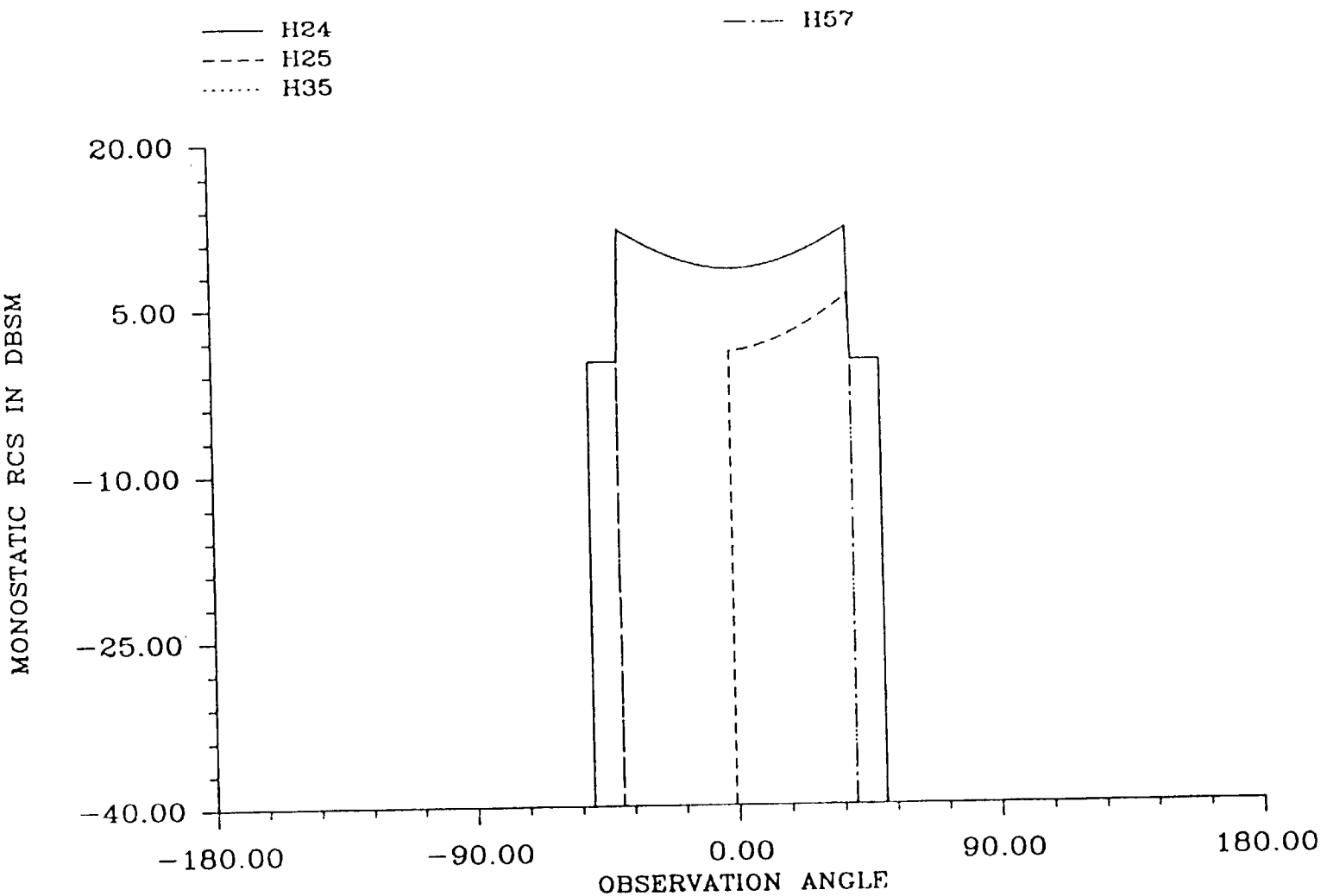

Fig. 14. Monostatic scattering components of a 90° dihedral corner reflector (soft polarization, $2\alpha = 90^{\circ}$, $\varepsilon_c = 7.8 - j1.6$, $\mu_c = 1.5 - j0.7$, $t = 0.052\ \lambda$, $A1 = A2 = B = 5.6088\ \lambda$).

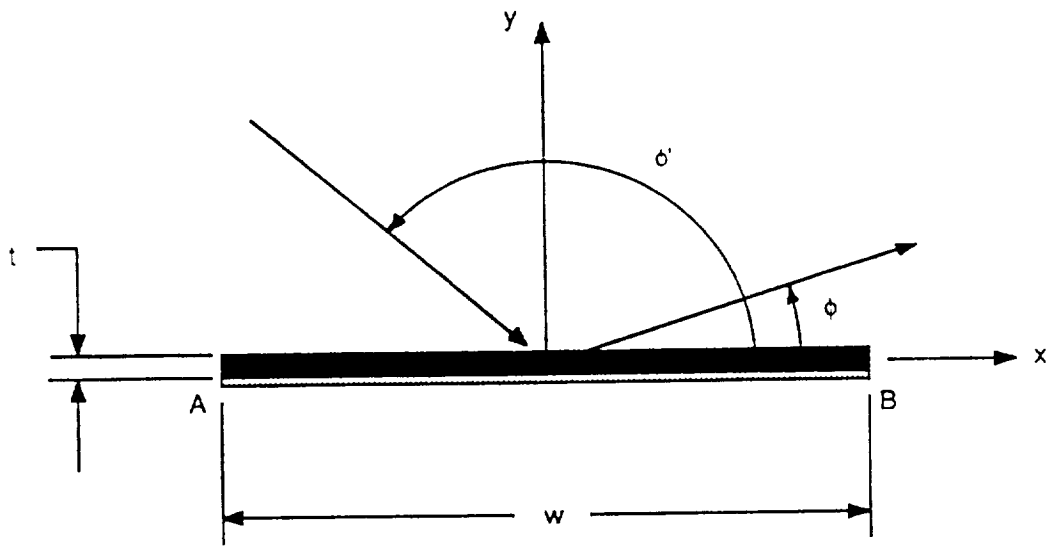

Fig. 15. Strip/plate geometry.

produce similar results, but they deviate considerably from each other away from normal incidence. For the soft polarization case of Fig. 16, both UTD models disagree with the FD-TD results away from normal incidence, indicating a need to include higher-order terms. Surface-wave terms, which are not included in this model, can be a significant contribution, expecially near grazing incidence. The need for surface-wave and higher-order terms is substantiated also by the hard polarization results of Fig. 17. The angularly varying impedance model produces improved results in the intermediary lobes. The discontinuity near grazing incidence points to a need for surface-wave and higher-order terms, which will be investigated in the future.

III. FUTURE WORK

The dearth of research in the area of scattering from coated geometries makes this an obvious focus of future investigation. Specifically, the angularly dependent equivalent surface impedance for the coated dihedral corner reflector will be incorporated into the present analysis. Additionally, surface-wave and higher-order terms will be added to the coated strip/plate model to study their effects, which should be significant near grazing incidence.

Another area of future research is the continuation of investigation into the nonprincipal-plane scattering from perfectly conducting, rectangular plates. Previous reports [30], [32], [33] detail several different modeling schemes, including various equivalent currents methods and corner diffraction coefficients.

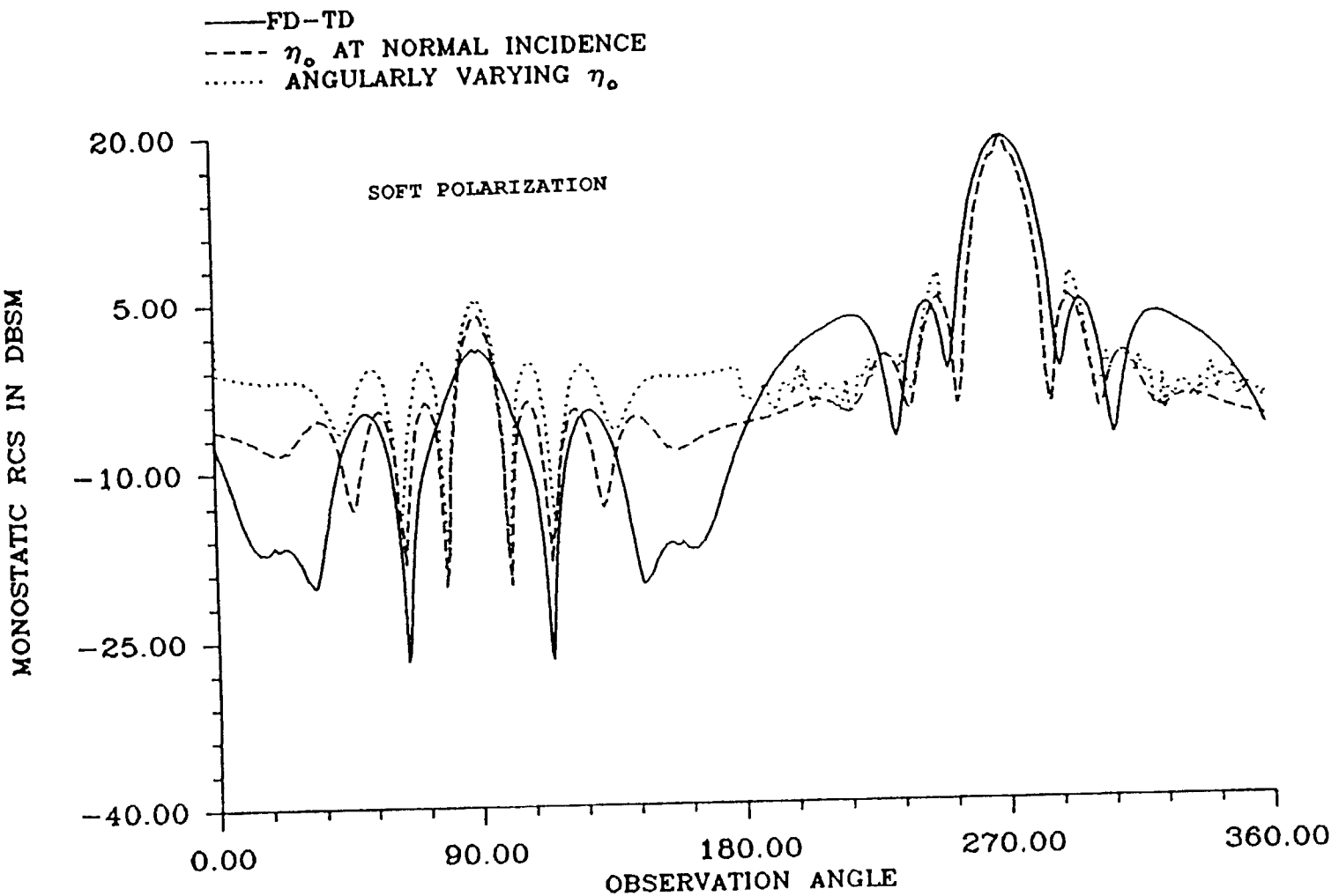

Fig. 16. Monostatic RCS of a coated square plate (w = 1.5 λ, coating: t = 0.065 λ, μ_c = 1.5 - j0.7, ε_c = 7.8 - j1.6).

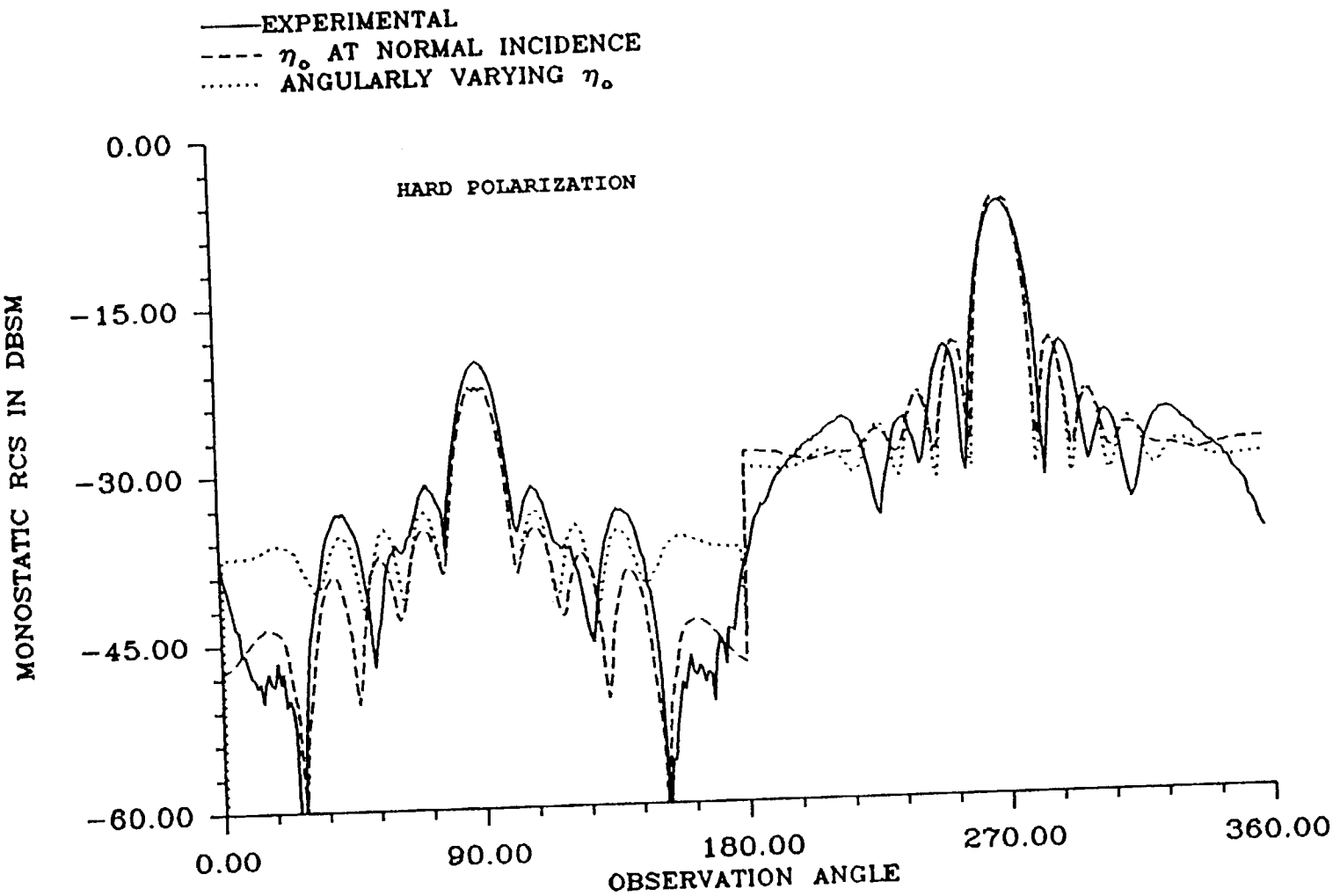

Fig. 17. Monostatic RCS of a coated square plate (w = 2.0 λ, coating: t = 0.0423 λ, μ_c = 2.12 - j1.5, ε_c = 10.2 - j3.8).

Results near and at normal incidence are accurate; however, near grazing incidence, the need for more terms is obvious. Specifically, third-order terms and more accurate corner diffraction terms seem necessary. Recently, Hansen [34] formulated a promising corner diffraction coefficient by comparing MM and Physical Theory of Diffraction (PTD) results for the scattering from a plate. This corner diffraction coefficient will be incorporated into our present plate models and reported on in the future.

The ultimate goal of this research is to combine the work on lossy surfaces and plate diffraction to obtain a comprehensive model for scattering from coated plates. Bistatic scattering and grazing-incidence scattering are important to consider in this model. The accurate high-frequency modeling of the rectangular plate at all angles of incidence and observation and the accurate characterization of the effects of a finite-thickness coating are crucial to the modeling of more complex targets.

IV. REFERENCES

[1] J. B. Keller, "Geometrical theory of diffraction," *J. Opt. Soc. Amer.*, vol. 52, pp. 116-130, Feb. 1962.

[2] R. G. Kouyoumjian and P. H. Pathak, "A uniform geometrical theory of diffraction for an edge in a perfectly conducting surface," *Proc. IEEE*, vol. 62, pp. 1448-1461, Nov. 1974.

[3] C. E. Ryan, Jr., and L. Peters, Jr., "Evaluation of edge-diffracted fields including equivalent currents for the caustic regions," *IEEE Trans. Antennas Propagat.*, vol. AP-17, pp. 292-299, Mar. 1969.

[4] ——, "Correction to 'Evaluation of edge-diffracted fields including equivalent currents for the caustic regions'," *IEEE Trans. Antennas Propagat.*, vol. AP-18, p. 275, Mar. 1970.

[5] A. Michaeli, "Equivalent edge currents for arbitrary aspects of observation," *IEEE Trans. Antennas Propagat.*, vol. AP-32, pp. 252-258, Mar. 1984.

[6] ——, "Correction to "Equivalent edge currents for arbitrary aspects of observation'," *IEEE Trans. Antennas Propagat.*, vol. AP-33, p. 227, Feb. 1985.

[7] ——, "Elimination of infinities in equivalent edge currents, part I: fringe current components," *IEEE Trans. Antennas Propagat.*, vol. AP-34, pp. 912-918, July 1986.

[8] ——, "Elimination of infinities in equivalent edge currents, part II: physical optics components," *IEEE Trans. Antennas Propagat.*, vol. AP-34, pp. 1034-1037, Aug. 1986.

[9] ——, "Equivalent currents for second-order diffraction by the edges of perfectly conducting polygonal surfaces," *IEEE Trans. Antennas Propagat.*, vol. AP-35, pp. 183-190, Feb. 1987.

[10] R. A. Shore and A. D. Yaghjian, "Incremental diffraction coefficients for planar surfaces," *IEEE Trans. Antennas Propagat.*, vol. AP-36, pp. 55-70, Jan. 1988.

[11] G. D. Maliuzhinets, "Excitation, reflection and emission of surface waves from a wedge with given face impedances," *Sov. Phys. Dokl.*, vol. 3, pp. 752-755, 1958.

[12] J. J. Bowman, "High-frequency backscattering from an absorbing infinite strip with arbitrary face impedances," *Canadian Journal of Physics*, vol. 45, pp.2409-2430, 1967.

[13] R. Tiberio, F. Bessi, G. Manara, and G. Pelosi, "Scattering by a strip with two face impedances at edge-on incidence," *Radio Science*, vol. 17, pp. 1199-1210, Sept.-Oct. 1982.

[14] R. Tiberio and R. G. Kouyoumjian, "A uniform GTD solution for the diffraction by strips illuminated at grazing incidence," *Radio Science*, vol. 14, pp. 933-941, Nov.-Dec. 1979.

[15] ——, "Calculation of the high-frequency diffraction by two nearby edges illuminated at grazing incidence," *Radio Science*, vol. 17, pp. 323-336, Mar.-Apr. 1982.

[16] ——,"Calculation of the high-frequency diffraction by two nearby edges illuminated at grazing incidence," *IEEE Trans. Antennas Propagat.*, vol. AP-32, pp. 1186-1196, Nov. 1984.

[17] R. Tiberio and G. Pelosi, "High-frequency scattering from the edges of impedance discontinuities on a flat plane," *IEEE Trans. Antennas Propagat.*, vol. AP-31, pp.590-596, July 1983.

[18] J. L. Volakis, "A uniform geometrical theory of diffraction for an imperfectly conducting half-plane," *IEEE Trans. Antennas Propagat.*, vol. AP-34, pp. 172-180, Feb. 1986.

[19] T. B. A. Senior and J. L. Volakis, "Scattering by an imperfect right-angled wedge," *IEEE Trans. Antennas Propagat.*, vol. AP-34, pp. 681-689, May 1986.

[20] J. L. Volakis and T. B. A. Senior, "Diffraction by a thin dielectric half-plane," *IEEE Trans. Antennas Propagat.*, vol. AP-35, pp. 1483-1487, Dec. 1987.

[21] M. I. Herman and J. L. Volakis, "High-frequency scattering by a resistive strip and extensions to conductive and impedance strips," *Radio Science*, vol. 22, pp. 335-349, May-June 1987.

[22] J. L. Volakis, "High-frequency scattering by a thin material half plane and strip," *Radio Science*, vol. 23, pp. 450-462, May-June 1988.

[23] R. Tiberio, G. Pelosi, and G. Manara, "A uniform GTD formulation for the diffraction by a wedge with impedance faces," *IEEE Trans. Antennas Propagat.*, vol. AP-33, pp. 867-873, Aug. 1985.

[24] T. Griesser and C. A. Balanis, "Reflections, diffractions, and surface waves for an interior impedance wedge of arbitrary angle," *IEEE Trans. Antennas Propagat.*, vol. AP-37, pp. 927-935, July 1988.

[25] C. A. Balanis, T. Griesser, and K. Liu, "Scattering patterns of dihedral corner reflectors with impedance surface impedances," Semiannual Report, Grant No. NAG-1-562, National Aeronautics and Space Administration, Langley Research Center, Hampton, VA, July 31, 1988.

[26] T. Griesser, C. A. Balanis, and K. Liu, "RCS analysis and reduction for lossy dihedral corner reflectors," *Proc. IEEE*, vol. 77, pp. 806-814, May 1989.

[27] E. H. Newman and M. R. Schrote, "An open surface integral formulation for electromagnetic scattering by material plates," *IEEE Trans. Antennas Propagat.*, vol. AP-32, pp. 672-678, July 1984.

[28] J. M. Jin and V. V. Liepa, "A numerical technique for computing TM scattering by coated wedges and half-planes," *Electromagnetics*, vol. 9, no. 2, pp.201-213, 1989.

[29] T. B. A. Senior, "Diffraction by a right-angled second order impedance wedge," *Electromagnetics*, vol. 9, no. 3, pp. 313-330, 1989.

[30] C. A. Balanis, L. A. Polka, and K. Liu, "Nonprincipal-plane scattering from rectangular plates and pattern control of horn antennas," Semiannual Report, Grant No. NAG-1-562, National Aeronautics and Space Administration, Langley Research Center, Hampton, VA, Jan. 31, 1990.

[31] T. Griesser, "High-frequency electromagnetic scattering from imperfectly conducting structures," Ph.D. dissertation, Arizona State University, Tempe, AZ, Aug. 1988.

[32] C. A. Balanis, L. A. Polka, and K. Liu, "Nonprincipal-plane scattering from flat plates — second-order and corner diffraction and pattern control of horn antennas," Semiannual Report, Grant No. NAG-1-562, National Aeronautics and Space Administration, Langley Research Center, Hampton, VA, July 31, 1989.

[33] C. A. Balanis, L. A. Polka, and K. Liu, "Nonprincipal plane scattering of flat plates and pattern control of horn antennas," Semiannual Report, Grant No. NAG-1-562, National Aeronautics and Space Administration, Langley Research Center, Hampton, VA, Jan. 31, 1989.

[34] T. B. Hansen, "Corner diffraction coefficients for the quarter plane," *IEEE Trans. Antennas Propagat.*, submitted for publication, July 1990.

PART B

ANTENNA PATTERN CONTROL USING IMPEDANCE SURFACES

ABSTRACT

This is the semiannual progress report for the *Antenna Pattern Control Using Impedance Surfaces* research grant. This report covers the research period from February 1, 1990 to July 31, 1990.

During this research period, we have developed the capacity to measure the electromagnetic properties of lossy materials. We have also investigated the effects of using multiple material coatings on the radiation pattern of the horn antenna. Numerous computations have been devoted toward the inverse problem of synthesizing desired radiation patterns using the impedance surfaces. Stabilizing the equivalent sheet impedance using the linear control condition has been attempted, and it has been found to be a very difficult task. A detailed review of the method has been performed. Corrective measures and alternative methods have been studied, and they are under review for implementation.

I. INTRODUCTION

A. Measurement of the Properties of the Lossy Materials

In this research period, we felt a great need (because of the lack of data from the manufacturers) for the measurement of the electrical properties of the lossy materials which we introduced to control the radiation pattern of the horn antenna. The accurate values of the complex permittivity and permeability are needed both in the realization of the horn antenna radiation pattern control and in the analysis of the horn antennas with impedance walls. While time consuming computations are queuing in the computer, a significant portion of our time was devoted to developing the capability to measure the electrical properties of lossy materials. Since the lossy materials used in the antenna's radiation pattern control are of solid type and have relatively high loss, the measurement of the complex permittivity (ε_r) and complex permeability (μ_r) can be performed with very good accuracy with the S-parameter method utilizing the HP8510 network analyzer[1],[2]. Figure 1 shows the configuration of the X-band waveguide sample holder in the testing system.

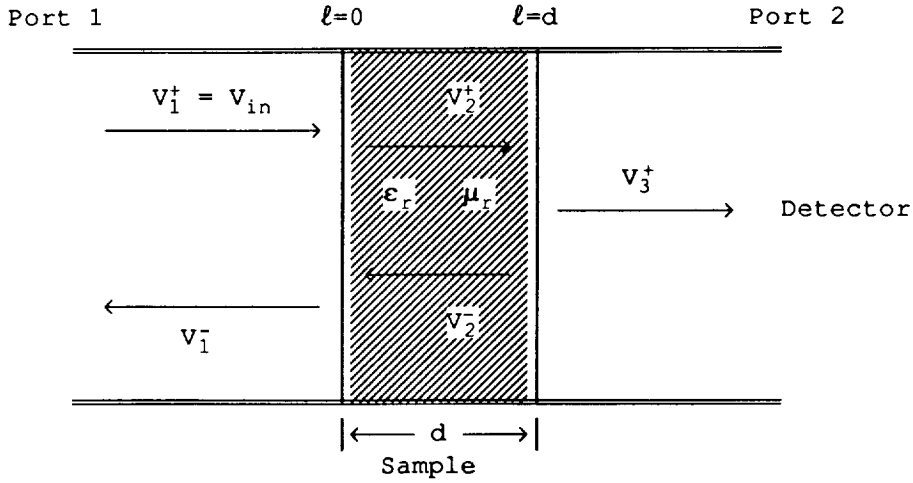

Figure 1. Configuration of the sample holder

In the S-parameter method, the mismatches in the feeding source and the load can be calibrated by the HP8510 calibration process. The effect of the higher order modes introduced by the insertion of the lossy material sample can be reduced to a negligible level if the sample is located far away (a few guided wavelengths) from the two coaxial waveguide adapters. Thus, by solving the boundary conditions at $\ell=0$ and $\ell=d$ using the transmission line model, the relationship between the S-parameters and the electrical properties of the sample can be found.

$$S_{11}(\omega) = \frac{V_1^-}{V_1^+}\bigg|_{\ell=0} = \frac{(1 - T^2)\Gamma}{1 - T^2\Gamma^2} \tag{1}$$

$$S_{21}(\omega) = \frac{V_3^+\big|_{\ell=d}}{V_1^+\big|_{\ell=0}} = \frac{(1 - \Gamma^2)T}{1 - T^2\Gamma^2} \tag{2}$$

where

$$\Gamma = \frac{\sqrt{\frac{\mu_r}{\varepsilon_r}} - 1}{\sqrt{\frac{\mu_r}{\varepsilon_r}} + 1} \tag{3}$$

$$T = \exp\left(-j\frac{2\pi}{\Lambda}\, d\right) \tag{4}$$

$$\Lambda = \frac{1}{\sqrt{\frac{\varepsilon_r\mu_r}{\lambda_o^2} - \frac{1}{\lambda_c^2}}} \tag{5}$$

where λ_o = free space wavelength, λ_c = cutoff wavelength of the X-band waveguide sample holder. From equation (1)-(4), the T and Γ can be obtained by

$$\Gamma = K \pm \sqrt{K^2 - 1} \tag{6}$$

$$T = \frac{S_{11}(\omega) + S_{21}(\omega) - \Gamma}{1 - [S_{11}(\omega) + S_{21}(\omega)]\Gamma} \tag{7}$$

where

$$K = \frac{[S_{11}^2(\omega) - S_{21}^2(\omega)] + 1}{2S_{11}(\omega)} \tag{8}$$

Using the measured $S_{11}(\omega)$ and $S_{21}(\omega)$, Γ, T, and Λ can be computed by using (6), (8), and (4). Then, using (3) and (5), the electrical properties of the lossy material in the X-band waveguide sample holder can be calculated using

$$\mu_r = \frac{1 + \Gamma}{\lambda_o(1-\Gamma)\sqrt{\frac{1}{\Lambda^2} + \frac{1}{\lambda_c^2}}} \tag{9}$$

$$\varepsilon_r = \frac{\lambda_o^2 \left[\frac{1}{\Lambda^2} + \frac{1}{\lambda_c^2}\right]}{\mu_r} \tag{10}$$

Since the measurement of S-parameters in HP8510 can be performed to cover the entire X-band, the material properties in X-band are obtained by the above formulas. This measurement system has been automated.

B. Theoretical Development of the Synthesis Problem

A systematical effort has been devoted toward the inverse problem. Special attentions have been paid to obtain a physically realizable sheet impedance distribution so that the inverse problem can be experimentally realized. However, this has been found to be a formidable task, and we have not yet obtained a stable inverse

solution of the impedance surface for a desired radiation pattern. The analysis of the synthesis method leads us to believe that the following reasons have contributed to the instabilities.

1. Non-Uniqueness of the Solution

Referring to Figure 2, the required aperture distribution $\mathbf{M}_2$ of the desired radiation pattern is to be realized by the control surfaces which are located in different locations. Therefore, there is no one-to-one correspondence between the control units and the desired aperture distribution. There are infinite many combinations of control surface impedances which could lead to the desired aperture distribution. The linear control condition allows a linear solution of the control equation. The numerical error in the solution of the electric currents due to the finite size of the segments on the control surface and the rapid changes of the desired aperture distribution seem to encourage the instability of the solution based on the linear control condition.

2. Solution of the Transition Equation

In the previous progress report, the horn antenna problem is outlined by Figure 2. In region 1 of Figure 2, the full-wave transition technique is developed to analytically compute the transmitted and reflected waves when this portion of the walls is of perfectly conducting surfaces. This technique is based on the same boundary condition as [3]. However, instead of approximating the continuous horn transition with a number of stepped rectangular waveguides, we formulate a set of first-order differential equations to analytically account for such a continuous transition.

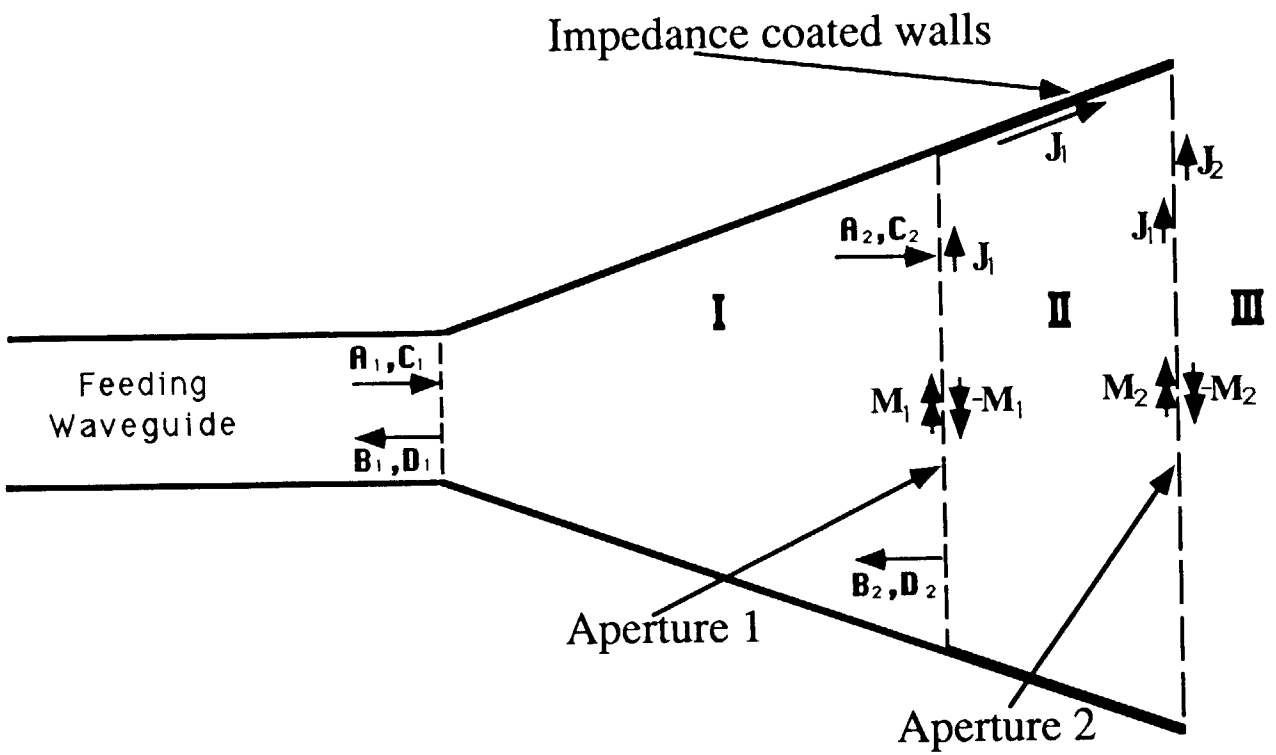

Figure 2. The equivalent problem of a horn antenna.

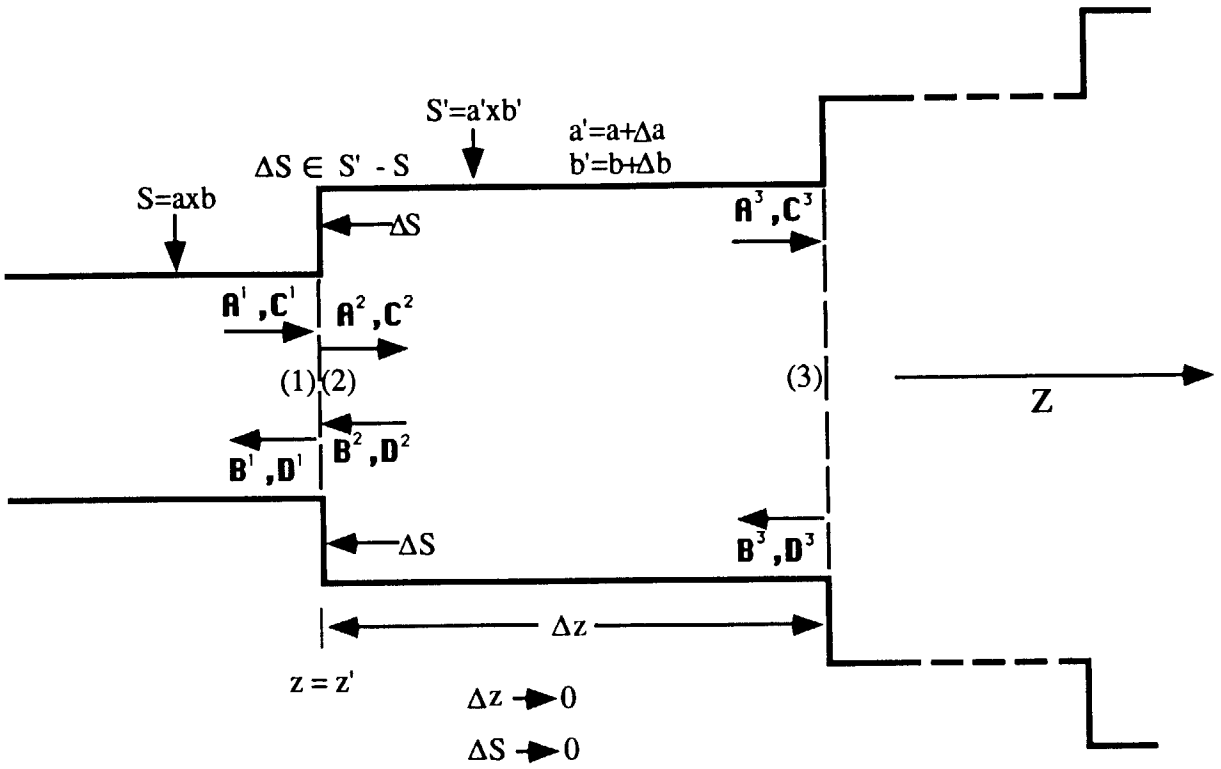

Figure 3. Differential model of the continuous horn transition.

For a horn transition, the problem can be viewed as a cumulated effect of the infinitely small stepped transitions of the rectangular waveguides as illustrated in Figure 3, where $\mathcal{A}$, $\mathcal{B}$, $\mathcal{C}$, and $\mathcal{D}$ are the full-wave expansion coefficients. Since the pyramidal horn has a continuous transition, its full-wave expansion coefficients are also continuous. Therefore, we can formulate a set of first-order differential equations in terms of their $\mathcal{ABCD}$ parameters which can be represented in the form of a matrix equation as follows:

$$\frac{d\mathbf{y}(z)}{dz} = \mathbf{T}(z)\cdot\mathbf{y}(z) \tag{11}$$

where

$$\mathbf{y}(z) = \begin{bmatrix} \mathcal{A} \\ \mathcal{B} \\ \mathcal{C} \\ \mathcal{D} \end{bmatrix} \tag{11a}$$

and $\mathbf{T}(z)$ is the two-port system matrix of the transition. The solution of (11) takes the general form of

$$\mathbf{y}(z_2) = e^{\mathbf{S}} \cdot \mathbf{y}(z_1) \tag{12}$$

where

$$\mathbf{S} = \int_{z_1}^{z_2} \mathbf{T}(z)\,dz \tag{13}$$

and

$$e^{\mathbf{S}} = \mathbf{I} + \mathbf{S} + \frac{\mathbf{S}^2}{2!} + \frac{\mathbf{S}^3}{3!} + \cdots\cdots \tag{14}$$

In (14), $\mathbf{I}$ represents the unit matrix. Such a solution is a very tempting one which is an analogy to the scalar differential equation.

Unfortunately, the solution in (13) is valid for only a few cases, for example when **S**(z) is diagonal or **S**(z) is independent of z[4],[5]. We have just realized such a constraint. Since this solution affects the computer program for both the analysis and the synthesis, alternative methods for such a solution are under implementation.

II. ACCOMPLISHMENTS

A. Measurements of the Properties of the lossy materials

The S-parameter method with the HP8510 network analyzer has been used in a series of measurements of the electrical properties of lossy materials. To show the accuracy of such a measuring system, a nylon sample was first used to perform the measurements. Figures 4 and 5 show, respectively, the real parts of the complex ε_r and μ_r of nylon (imaginary parts are negligibly small, and they are omitted) at X-band. As shown in the figures, our measured values are within the second decimal point accuracy compared to the well-known values of nylon (ε_r=3.0, μ_r=1). Next, we proceeded to measure material properties of two surface-wave absorbing materials which are suited for the radiation pattern control of the horn. The first is the Eccosorb-GDS. Figures 6 and 7 show, respectively, the real and imaginary parts of ε_r and μ_r for the material. These values differ from those published in [6], however; our measurements have shown very good repetition of the results. We believe that the batch difference of the sample might be the reason for such a difference. The second surface-wave absorbing material we measured was the SWAM (Surface Wave Absorbing Material). Figures 8 to 11 show, respectively, the measured data for real and imaginary parts of ε_r and μ_r for two measurements.

B. Theoretical Development of the Synthesis Problem

In the previous reports, we have demonstrated that the sheet impedance material can be effectively used to control the radiation pattern of the horn antenna. In this research period, the effect of multiple sheets of impedance coatings on the top and the bottom walls of the antenna has also been investigated. Figure 12 shows the comparison of the E-plane radiation patterns for conducting walls, a 1.5 cm GDS plus a 3 cm SWAM coating, and a 7.45 cm GDS coatings on the top and the bottom walls of the horn. The layout of the coating is shown on the insert of Figure 12. At a frequency of 10.1 GHz, the GDS material has a measured relative permittivity of 14.83-j0.06, and a relative permeability of approximately 1.47-j1.46. The SWAM material has a measured relative permittivity of 16.55-j0.47, and a relative permeability of approximately 1.50-j1.22 at the same frequency. These experimental results show that the combination of GDS and SWAM coating materials can achieve the same pattern control as that of 7.45cm GDS coating (eliminating the first sidelobe) while the pattern suffers a much smaller loss in its total gain(4.5dB for 7.45cm GDS and 2.1dB for the combined coating of GDS and SWAM).

Efforts have also been devoted to examining the source of the rapid ripples in the back lobes of the H-plane radiation pattern. To investigate this ripple structure, the surface-wave absorbing material SWAM has been used to coat on the outside surfaces of the horn antenna. Figure 13 shows the comparison of the H-plane radiation patterns. As expected, the coating of the surface wave absorbing material greatly reduces the magnitude of the rapid ripple pattern, which confirms our assumption that the diffraction of the outer

surface and the back structure of the horn antenna measuring device is one of the sources of these ripples. Also, as expected, since a portion of the diffracted energy is absorbed by the surface wave absorbing material, a much lower radiation is observed in the back region of the horn antenna.

III. FUTURE WORK

Experimentally, we have demonstrated the control of the impedance surfaces on the radiation pattern of the horn antenna. Theoretically, however, we have not yet realized a stable and practical surface impedance distribution on the inner surfaces of the horn antenna for a desired radiation pattern in the synthesis problem. In the next research period, the following efforts will be devoted to this research project.

a. Develop an alternate solution of the transition equation (11) using Runge-Kutta method [7] or other efficient numerical methods.

b. Investigate the sidelobe level control to approach the desired radiation pattern. As an example, Figure 14 shows a desired E-plane radiation pattern, which is the -90° to 90° portion of the H-plane pattern of the same horn antenna, and the synthesized pattern with the sidelobes being individually controlled by using modified Taylor's pattern synthesis[8],[9]. The sidelobe levels are set at -31 dB for the first sidelobe, -40 dB for the second sidelobe, and -42 dB for the third sidelobe. Figure 15 shows the comparison of the required aperture magnetic current distributions for the sidelobe level control and for the

variational pattern control proposed by the previous report (an equivalent null-free synthesis method by P. M. Woodward [10] may lead to a similar aperture distribution). It is demonstrated in Figure 15 that if instead of synthesizing every detail of the desired radiation pattern, we may be better off to control only its sidelobe levels to approach the desired pattern. If this is attempted, a much smoother aperture magnetic current distribution will be needed for the synthesis problem. Therefore, if the fine details of the radiation pattern outside the major lobes are not our major objective, a smoother aperture distribution can help to stabilize the solution of the control surface impedance. Moreover, this type of aperture distribution is more practical to be realized by using impedance surfaces on the walls of the horn antenna. Similar distributions have been achieved by using impedance walls of the parallel plate waveguide as demonstrated by [11]. Therefore, it is an option for us to work on.

c. From the realization point of view, since the sheet impedance solution based on the linear control condition varies from point to point, it is not a very practical way of realizing such a distribution. We are looking at the solution to the inverse problem in which the material parameters of the impedance coating changing only on the direction of the horn transition; i.e., the z-axis in Figure 3.

IV. PUBLICATIONS

During this reporting period, four papers have been submitted for publication in *IEEE Transaction on Antennas and Propagations*. Two of them have been accepted. One paper were presented in international symposium. The work reported in all of these papers was supported by this NASA grant. These are as follow:

a. Kefeng Liu and C. A. Balanis, "Simplified formulations for two-dimensional TE-polarization field computations," accepted to be published in *IEEE Trans. on Antennas and Propagat.*.

b. F. L. Whetten, Kefeng Liu and C. A. Balanis, "An efficient numerical integral in three-dimensional electromagnetic field computations," in *IEEE Trans. Antannas and Propagat.* to be published in September, 1990.

c. Kefeng Liu and C. A. Balanis, "Analysis of horn antennas with impedance walls," in *IEEE AP-S International Symposium Digest* (Dallas, TX) May 1990 pp. 1184-1187.

d. Kefeng Liu and C. A. Balanis, "Analysis of pyramidal horn antennas with or without impedance walls," submitted for publication in *IEEE Trans. on Antennas and Propagat.*.

e. Kefeng Liu and C. A. Balanis, "Near-field interaction between sinusoidal electric and magnetic dipoles," submitted for publication in *IEEE Trans. on Antennas and Propagat.*.

V. References

1. A. M. Nicolson and G. F. Ross, "Measurement of the intrinsic properties of materials by time domain techniques," *IEEE Trans. Instrum. Meas.*, Vol. IM-19, pp. 377-382, Nov., 1970.

2. William B. Weir, "Automatic measurement of complex dielectric constant and permeability at microwave frequencies," *Proc. IEEE*, Vol. 62, No. 1, Jan., 1974.

3. T. Wriedt, K. H. Wolff, F. Ardnt, and U. Tucholke, "Rigorous hybrid field theoretic design of stepped rectangular waveguide mode converters including the horn transitions into half-space," *IEEE Trans. Antennas Propagat.*, vol. AP-37, no.6, pp. 780-790, June, 1989.

4. P. M. Dersso, R. J. Roy, and C. M. Close, *State Variables for Engineers*, Wiley, 1965.

5. C. T. Chen, *Linear System Theory and Design.* Holt, Rinehart and Winston, 1984.

6. J. J. H. Wang, V. K. Tripp, and J. E. Tehan, "The magnetically coated conducting surface as a dual conductor and its application to antennas and microwaves," *IEEE Trans. Antennas Propagat.*, vol. AP-38, pp. 1069-1077, July, 1990.

7 J. C. Butcher, *Numerical Analysis of Ordinary Differential Equations.* Wiley, 1987.

8. R. S. Elliott, "Design of line-source antennas for sum patterns with sidelobes of individually arbitrary heights," *IEEE Trans. Antennas Propagat.*, vol. AP-24, pp. 66-83, Jan., 1976.

9. R. S. Elliott, *Antenna Theory and Design*, Prentice Hall, 1981.

10. P. M. Woodward, "A method of calculating the field over a plane aperture required to produce a given polar diagram," *J. IEE (London)*, pt. IIIA, vol. 94 (1947), 1554-1558.

11. C. M. Knop, Y. B. Cheng, and E. L. Ostertag, "An absorber-wall parallel plate waveguide," *IEEE Trans. Microwave Theory Tech.*, vol. MTT-34, pp. 761-766, July, 1986.

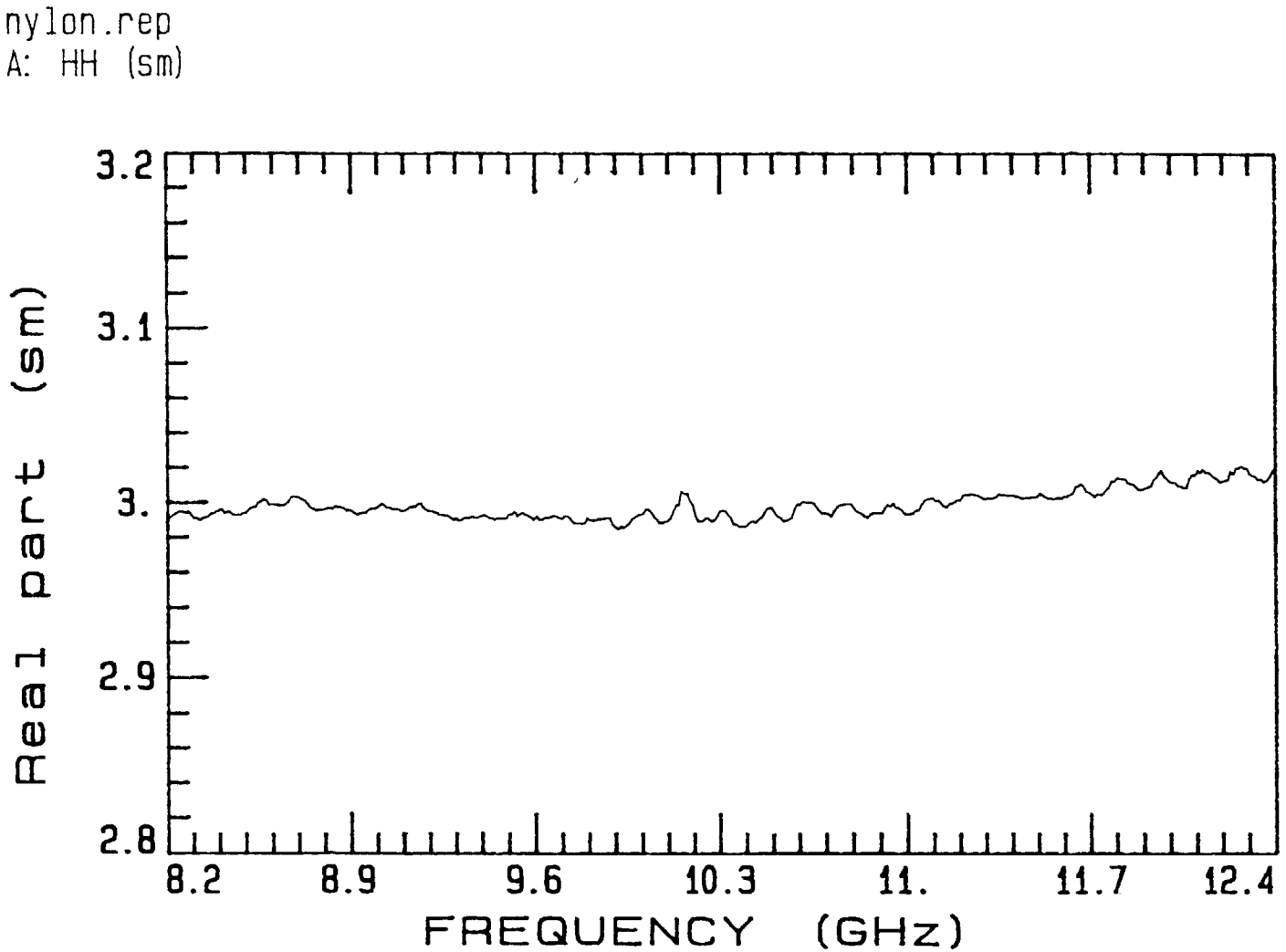

Figure 4. Real part of measured permittivity of nylon.

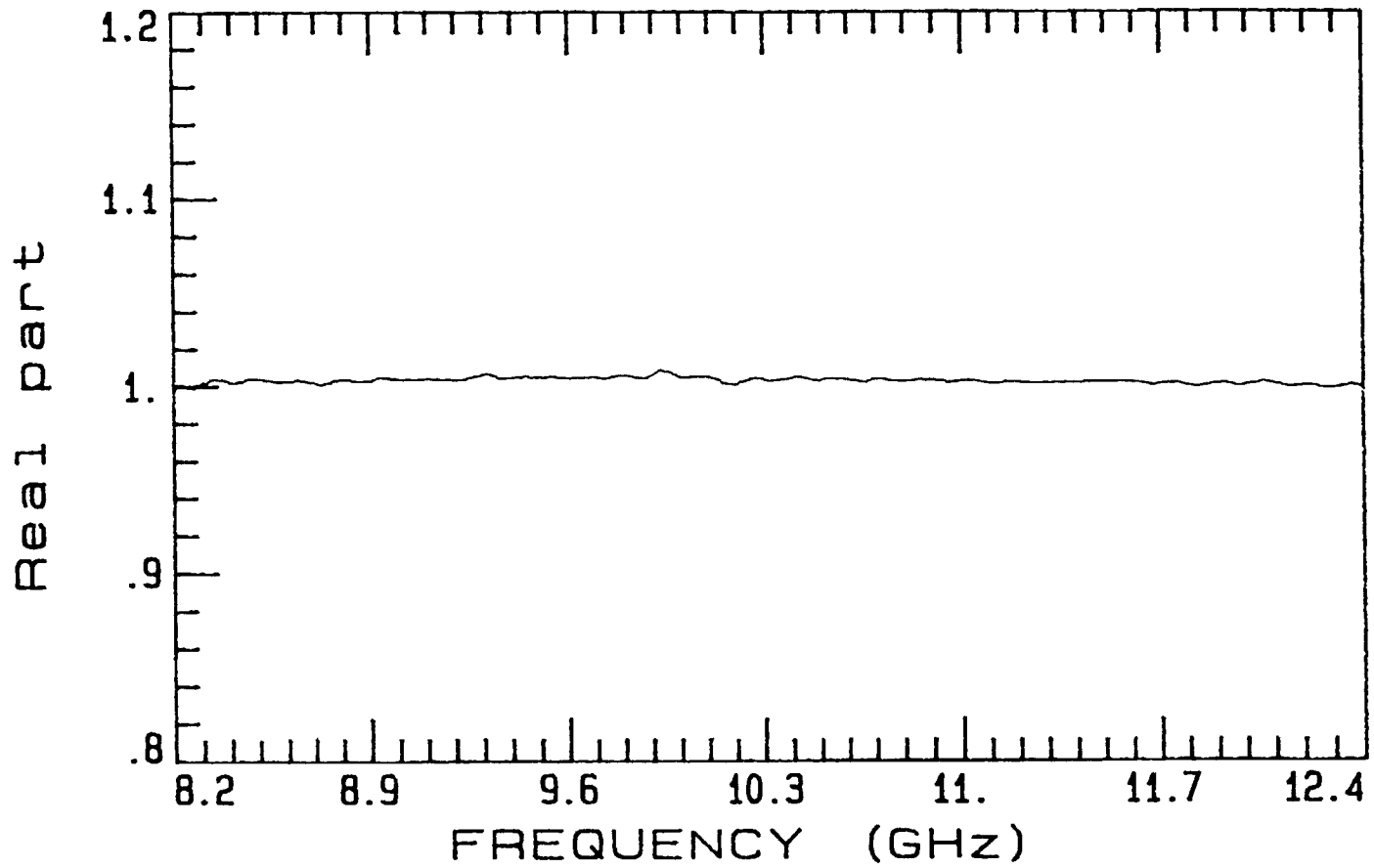

Figure 5. Real part of measured permeability of nylon.

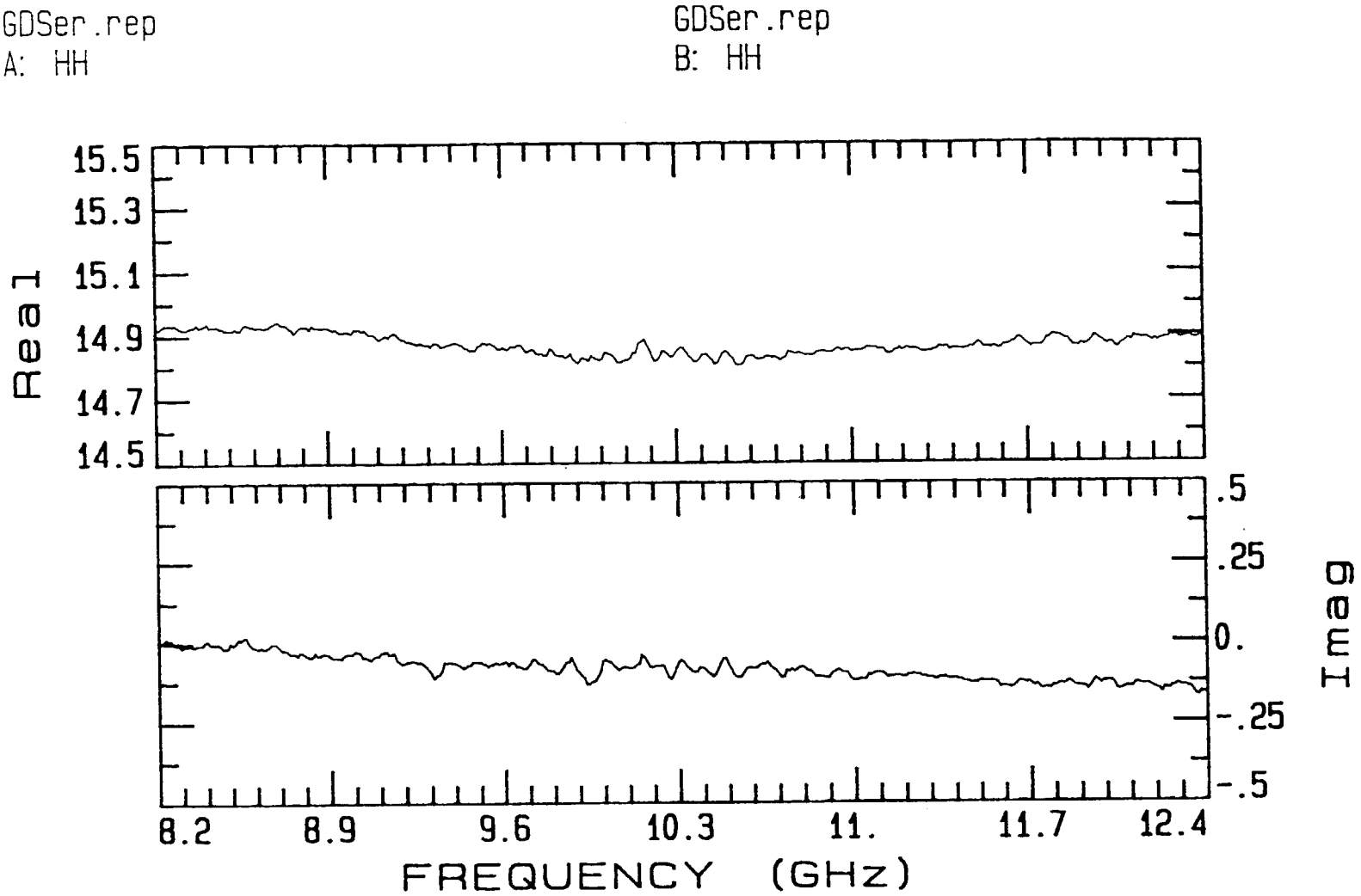

Figure 6. Complex permittivity of Eccosorb-GDS.

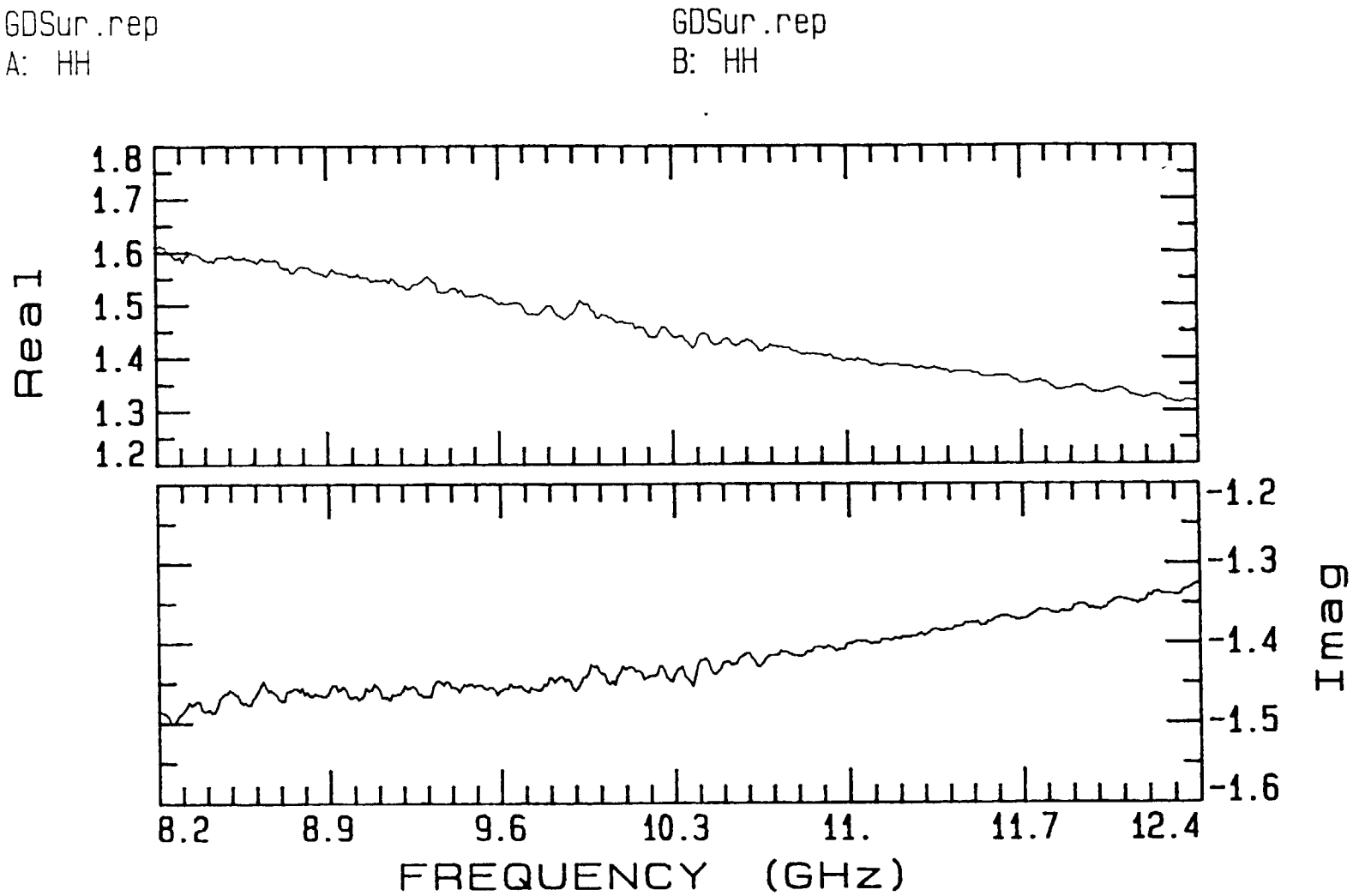

Figure 7. Complex permeability of Eccosorb-GDS.

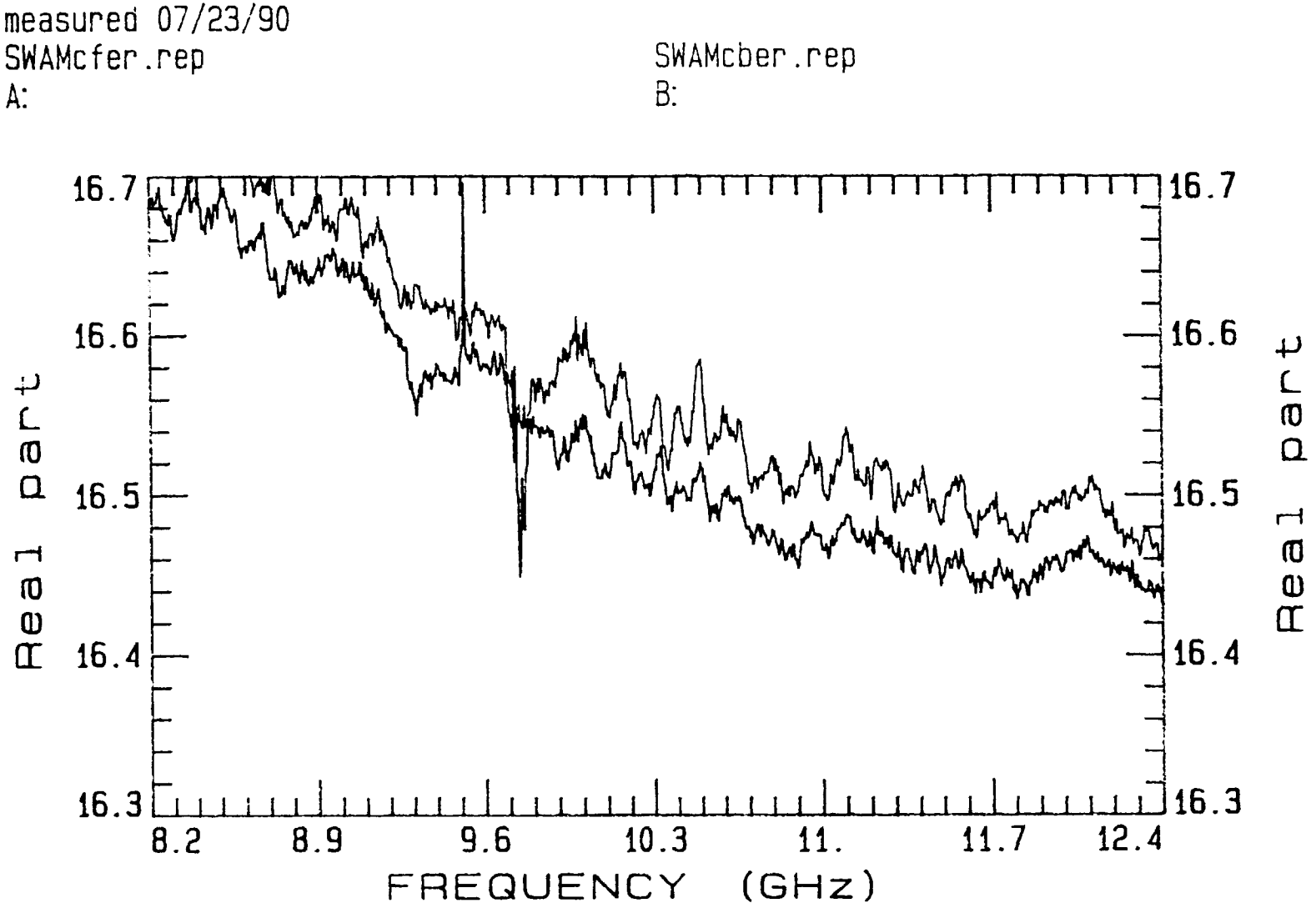

Figure 8. Two testing results of the real part of the permittivity of SWAM material.

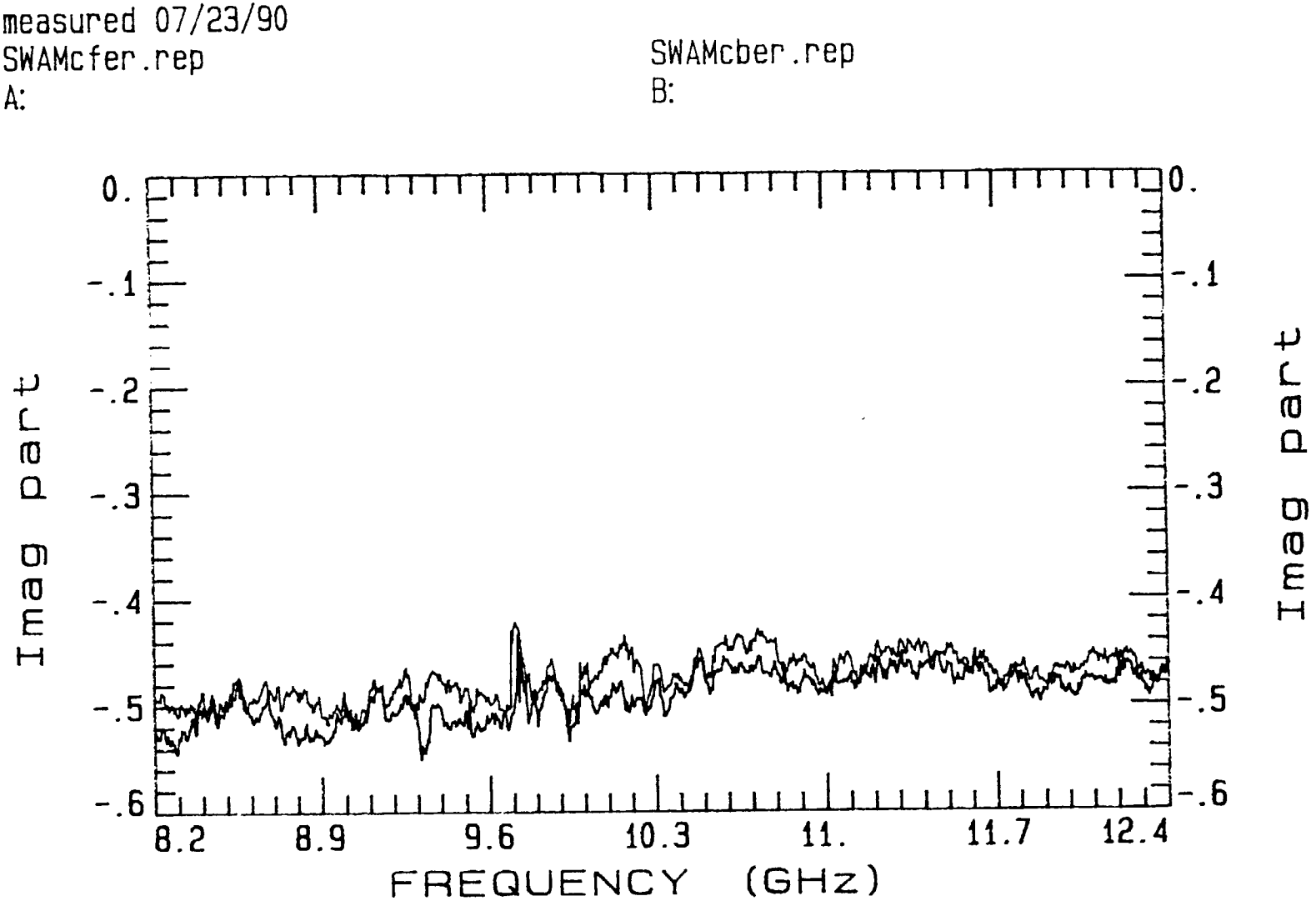

Figure 9. Two testing results of the imaginary part of the permittivity of the SWAM material.

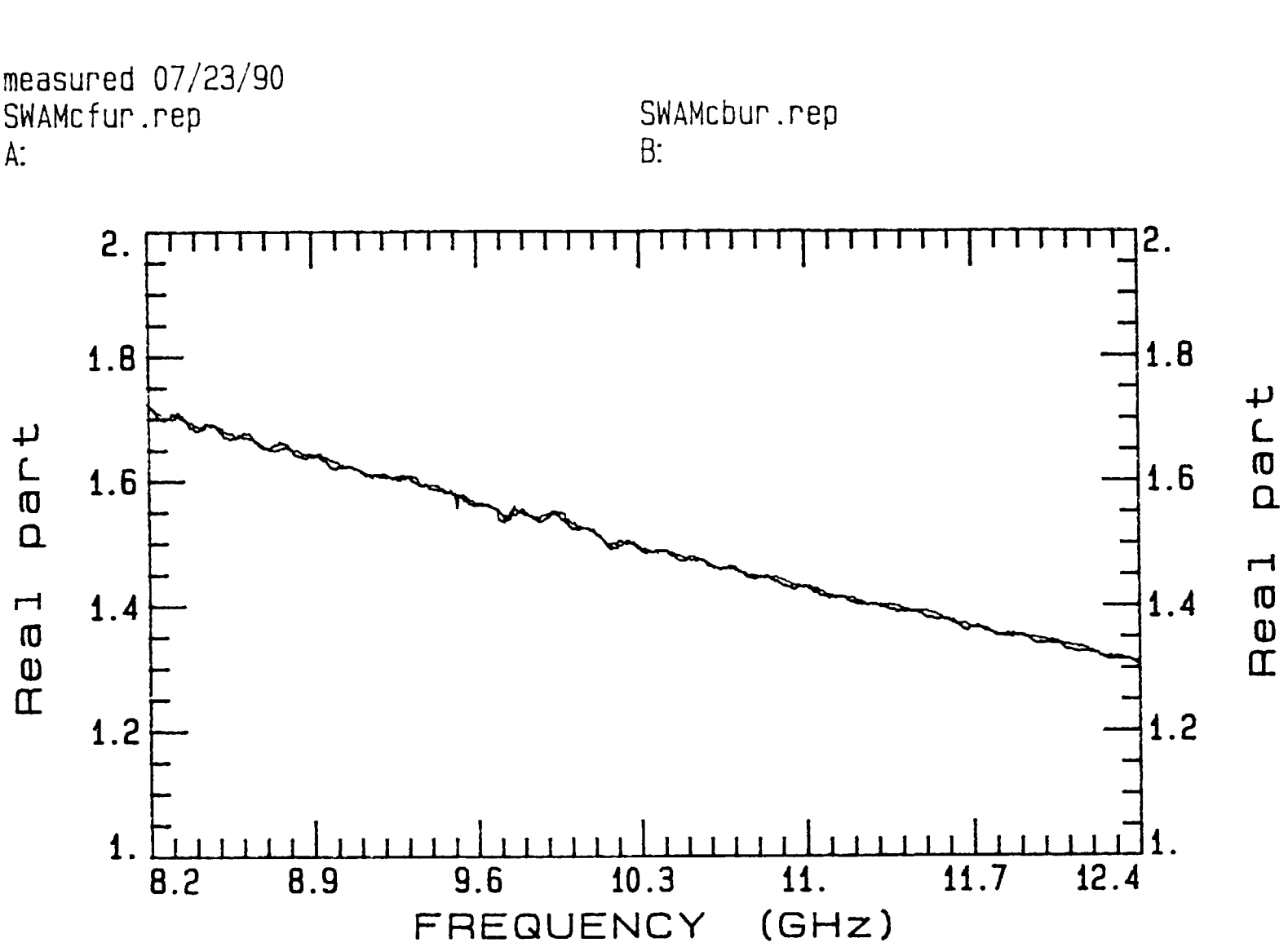

Figure 10. Two testing results of the real part of the permeability of the SWAM material.

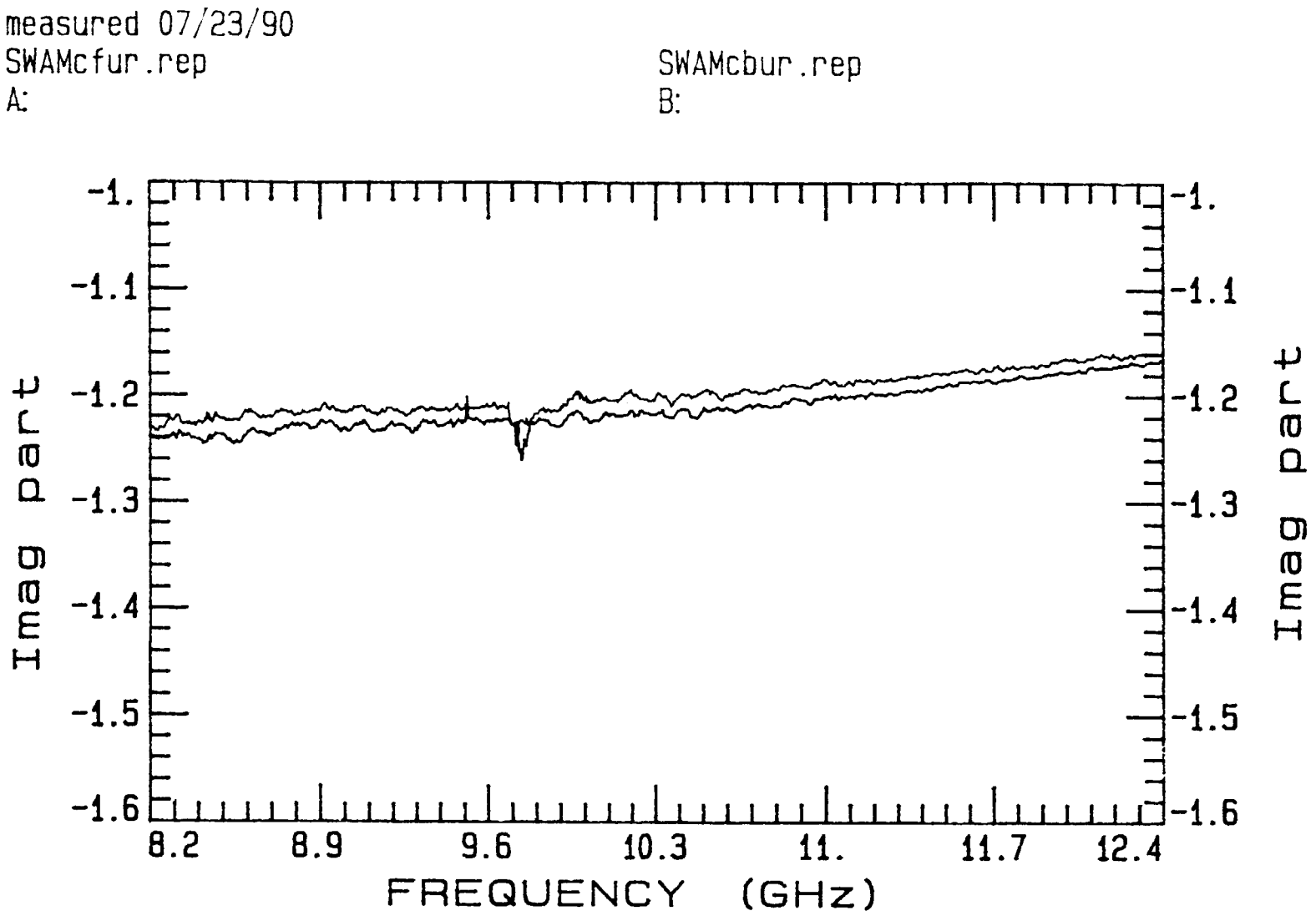

Figure 11. Two testing results of the imaginary part of the permeability of the SWAM material.

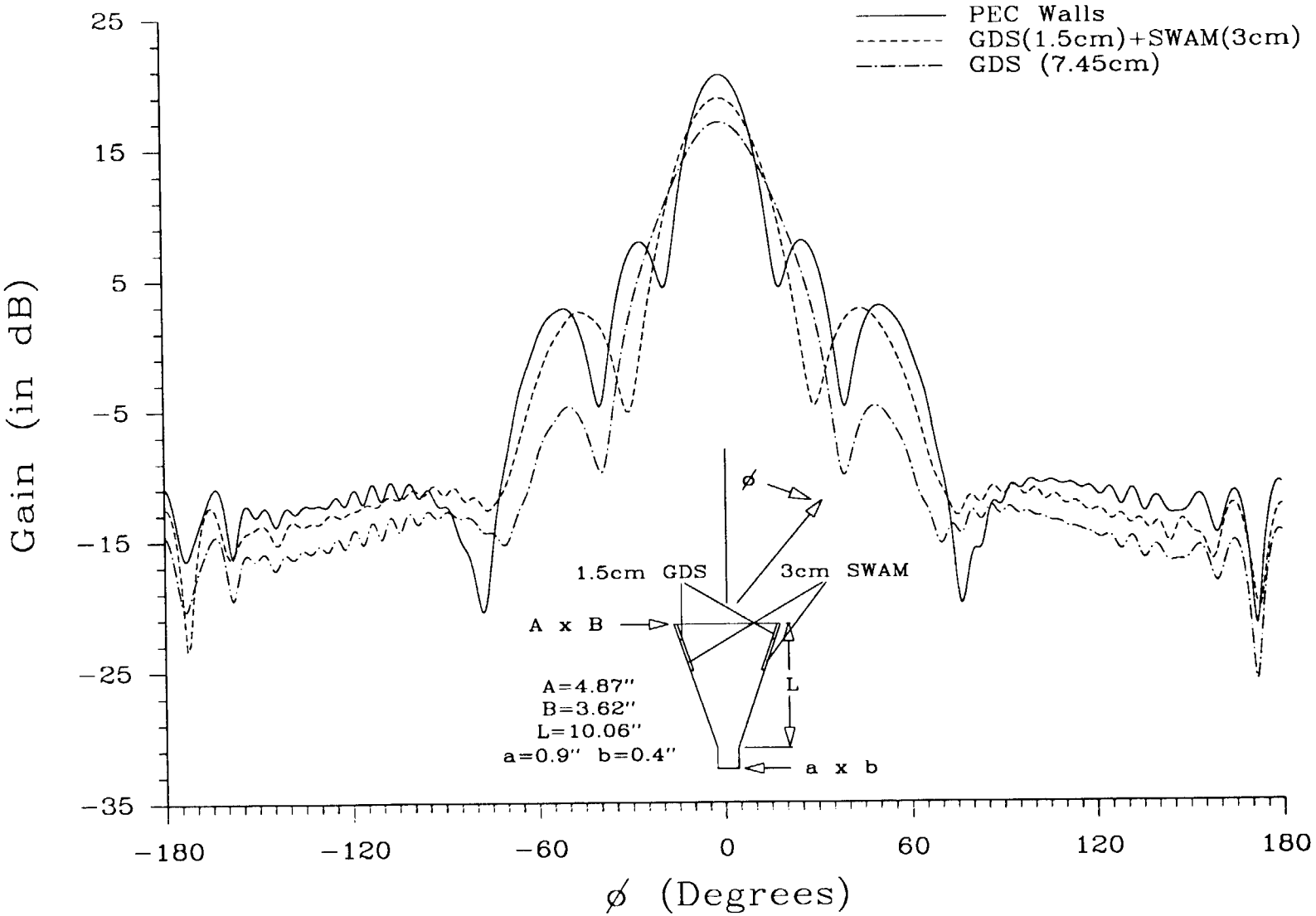

Figure 12. E−plane gain pattern of 20−dB horn at 10.1 GHz

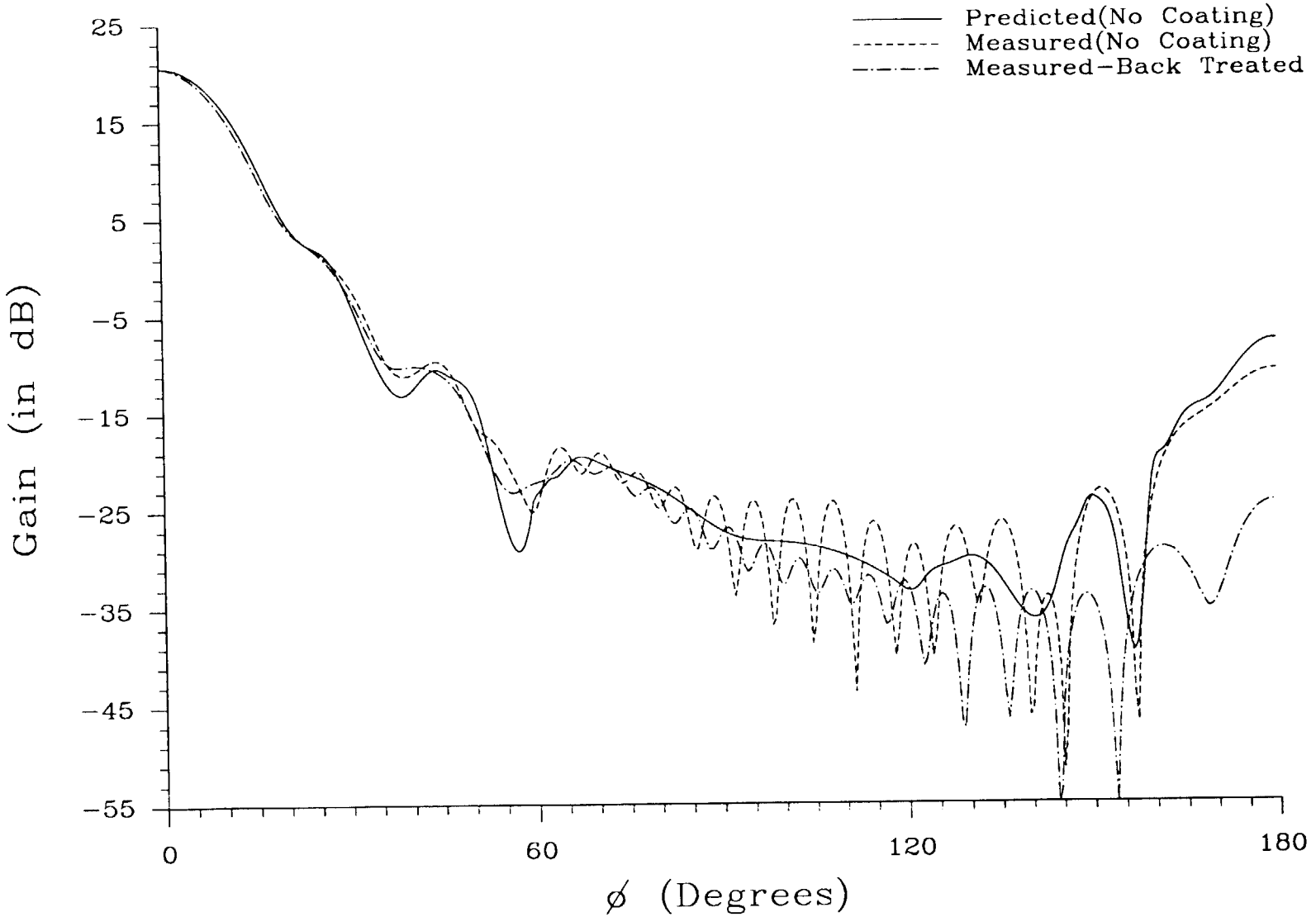

Figure 13. H-plane gain pattern for 20-dB horn at 10.1 GHz.

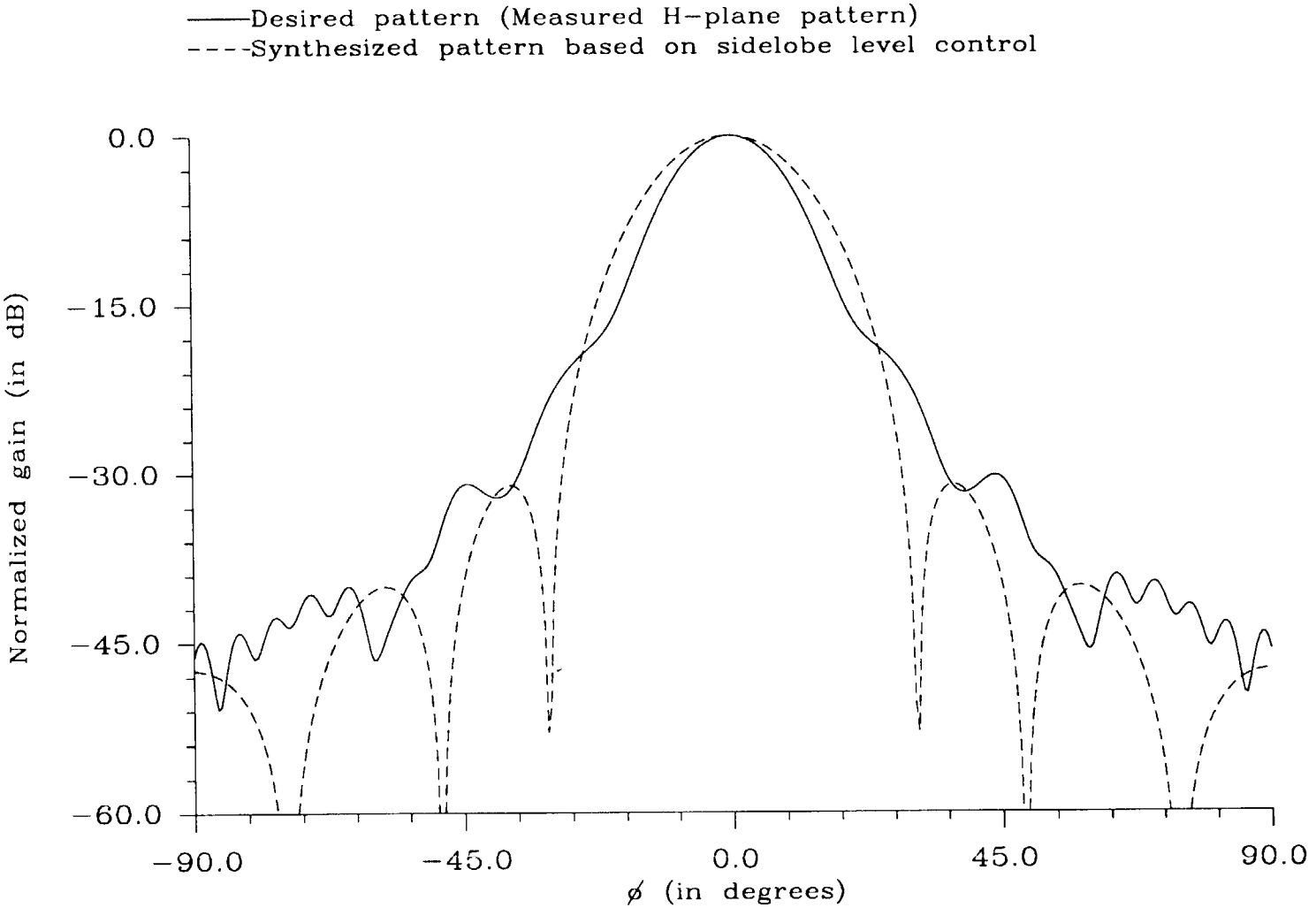

Figure 14. The desired pattern and the sidelobe level controlled pattern.

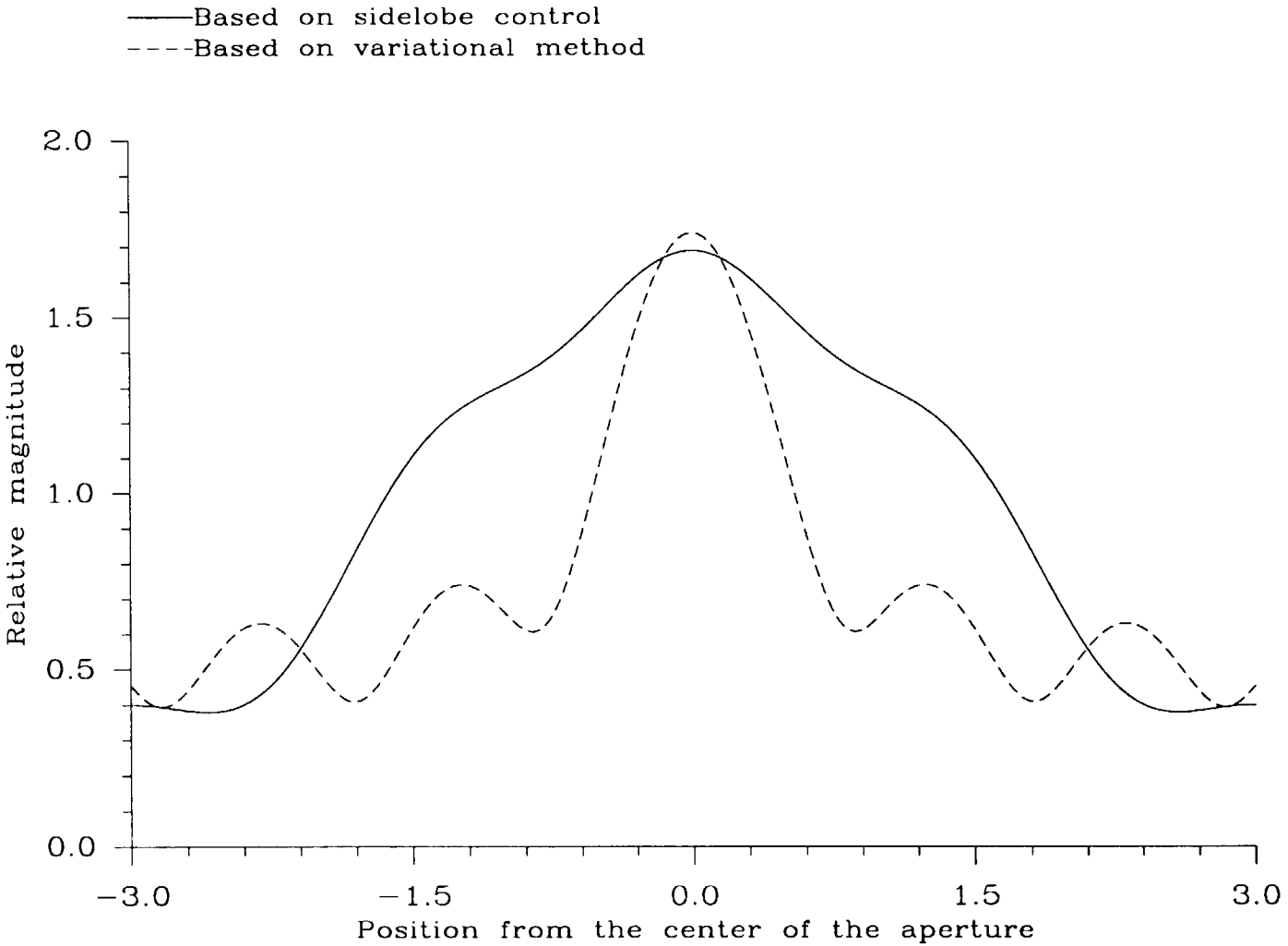

Figure 15. Comparison of required aperture magnetic current distributions from the two synthesis methods for the desired pattern in Figure 14.